Synthesis of Optical Nanodevices with Application in Biosensing

Wei Chen

A Thesis

In the Department

of

Electrical and Computer Engineering

Presented in Partial Fulfillment of the Requirements

For the Degree of Master of Applied Science

(Electrical and Computer Engineering) at

Concordia University

Montréal, Québec, Canada

December 2010

© Wei Chen, 2010

CONCORDIA UNIVERSITY

SCHOOL OF GRADUATE STUDIES

This is to certify that the thesis prepared

By: Wei Chen

Entitled: "Synthesis of Optical Nanodevices with Application in Biosensing"

and submitted in partial fulfillment of the requirements for the degree of

Master of Applied Science

Complies with the regulations of this University and meets the accepted standards with respect to originality and quality.

Signed by the final examining committee:

_____ Chair

Dr. D. Qiu

_____ Examiner, External

Dr. W. F. Xie, MIE To the Program

_____ Examiner

Dr. A. J. Al-Khalili

_____ Supervisor

Dr. M. Kahrizi

Approved by: _____

Dr. W. E. Lynch, Chair

Department of Electrical and Computer Engineering

_____20_____ _____

Dr. Robin A. L. Drew

Dean, Faculty of Engineering and

Computer Science

ABSTRACT

Synthesis of Optical Nanodevices with Application in Biosensing

Wei Chen

The unusual optical, magnetic, electronic, catalytic and mechanical properties of nanoparticles and nanoscale structure have been applied in many fields, especially in biology. A significant and unique phenomenon of nanoparticles or nanostructure, localized surface plasmon resonance (LSPR) was widely used in biosensor. A cost-effective and high-throughput technique to fabricate metal nanostructure arrays of various geometries on solid substrates was demonstrated. The nanostructure arrays were prepared through nanosphere lithography method. The fabrication involved self-assembly monolayer which was prepared by polystyrene microspheres and gold plasmon which was sputtered on top of the polystyrene monolayer. The nanostructures, triangular particles (with 920nm polystyrenes) and nanorings (with 420nm polystyrenes) which were obtained after the removal of polystyrene, distributed uniformly on a silanized glass substrate. The size of the nanorings or the distance between the triangular particles precisely corresponds to the footprint of the polystyrene microspheres that were in contact with the glass substrate before dissolution. However, in this research, no gold triangular particles were found with the polystyrene of 420nm in diameter and very few nanorings can be produced with the polystyrene of 920nm in diameter. Meanwhile, several methods to produce silver colloids were introduced as well.

Acknowledgements

First, I would like to thank my supervisor Professor Mojtaba Kahrizi, for giving me the opportunity and independence to pursue such an interesting thesis topic. Thank you for giving me the space to grow and learn in this domain.

I would also like to express my deepest appreciation to Dr. Simona Badilescu for her constant support and understanding. Without her support and encouragement, I could not have finished this thesis. I can not have the words to express my gratitude in helping me get through the difficult times and in encouraging me to strive to be a better researcher.

Many thanks to Mahmood Alimahmoode of the Civil/Environmental Engineering department in giving me training of the necessary equipment and in always finding the available time for the equipment.

Last but not least, I am very grateful to my father Chun Chen and my mother Jiang Shen for their continuous love and support throughout my life; I also would like to thank my Uncle Zheng Chen and my Aunt Bixia Zhao for taking care of me and giving me their unconditional love and support.

Table of Contents

List of Figures

List of Tables

List of Acronyms

APTES	3-Aminopropyltriethoxysilane
EBL	electron beam lithography
IBL	ion beam lithography
LED	light-emitting diodes
LSPR	localized surface plasmon resonance
NH_2	amino
NSL	nanosphere lithography
PPAs	Single-layer periodic particle arrays
PS	polystyrene
RIU	refractive index unit
SEM	scanning electron microscopy
SP	surface plasmon
SPR	surface plasmon resonance
TE	transverse electric of s-polarized
TM	transverse magnetic or p-polarized

UV	ultra violet
UV-vis	ultraviolet visible
XRL	X-ray lithography

List of Principal Symbols

a	The radium of the metallic Nanosphere
a_{ip}	In-plane diameter
b	The out-of-plane heights
C	Concentration of the colored compound
D	Nanosphere diameter
d	The effective thickness of the adsorbate layer
d_f	Waveguide thickness
d_{ip}	Interparticle spacing
d_m	Deposition mass thickness
E	Amplitude of electrical field
E (λ)	Extinction
g	Overall Gibbs free-energy density
$g_{sur\text{-}vac}$	Gibbs free-energy density between the bare surface and the vacuum outside
$g_{sur\text{-}lay}$	Gibbs free-energy density between the surface and the layers of adsorbed atoms

$g_{lay\text{-}vac}$	Gibbs free-energy between these layers and the vacuum
I	Intensity of the light transmitted through the sample
I_0	Intensity of transmitted light using the pure solvent
l_d	Characteristic electromagnetic-field-decay length
L	Distance of the light passes through the solution
K	Constant
K’	Constant
KC	Absorbance
M	Amplitude of magnetic field
m	The bulk refractive-index response of the nanoparticles
N	The effective refractive index
N_A	The area density of nanoparticles
n_c	The refractive index of sample media
Δn	The change in refractive index
P_s	Spreading pressure
r	Thickness of the nanoring wall
T	Transmittance of the solution

Δz	Penetration depth
λ	Wavelength
λ_{max}	The wavelength of the maximum absorbance or extinction maximum
$\Delta \lambda$	The shift in extinction maximum
ε	Fraction of the surface covered
ε_m	The dielectric constant of the medium around the metallic nanoparticles
ε_r	The real part of the metallic nanosphere's dielectric function
ε_i	The imaginary part of the metallic nanosphere's dielectric function
χ	The aspect ratio of nanoparticles

Chapter 1: Introduction

1.1 Nanotechnology

Nano is derived from the Greek word for dwarf, which depicts length in 10^{-9} meter. Those Materials, devices and structures, which can be regarded as being nanoscale must have at least one dimension less than 100nm. Nanotechnology is defined by the United States National Nanotechnology Initiative as [1]: "The understanding and control of matter at dimensions of roughly 1 to 100 nm, where unique phenomena enable novel applications".

After the term nanotechnology was firstly mentioned back in December 1959 by Richard Feynman in his visionary lecture named" There is plenty of room at the Bottom", nanotechnology has undergone significant development during these decades. Not only is nanotechnology involved in Physics and Engineering, it also encompasses in other disciplines, especially in Chemical and Biology.

Combined with the unique properties of nanomaterial, biomedical nanotechnology can be utilised in diagnostics, drug delivery, tissue engineering and so on. Genetic sequence can be detected by tagging gold nanoparticles with short segment of DNA; human will suffer less and spend less expense by using co-polymers, which hold small drug molecules and transport them to the desired location in body [2].

Nanotechnology can also be applied in boosting efficiency and reducing energy consumption. Compared to current light bulbs which only convert 5% of the electrical

energy into light, light-emitting diodes (LED), a kind of nanotechnology approach can greatly reduce the consumption of energy for illumination. Solar cells, which take advantage of nanotechnology, can greatly increase the efficiency of light conversion as well.

In addition, nanotechnology can be applied in heavy industry, such as aerospace, construction and vehicle manufacturering. However, a main difficulty of the development of nanotechnology is to figure out how to solve the problem of the need for cost-effective large-scale production method [2].

Numbers of applications in many fields can benefit from nanotechnology; however, some dangerous aspects might exist on our health and on our environmental. As the nanotechnology can produce all kinds of new, promising product and the sizes of these products are so tiny that may eventually cause the health problem for the customers. Therefore, considered the potential mass health problem, scientists must act responsibly and treat with caution when they apply nanotechnology on any research.

Despite these potential disadvantage and fear of nanotechnology, there is so much to expect from nanotechnology. Hence, various kinds of nanostructures are fabricated for this reason. Many methods are developed to fabricate nanomaterials, nanostructures and nanodevices; generally, these techniques are divided into top-down and bottom-up approaches. Top-down approach depicts those materials in bulk which are reduced into nanometer scale, while bottom-up approach demonstrates nano sized structures which are built up into complex structures by assembling molecule by molecule, or atom by atom.

The formation of self-assembled monolayer is one of the examples of bottom-up and the formation will be introduced in detail in the following chapter.

1.2 Nanostructure

Physical and chemical properties of the material can dramatically change as the sizes of materials are reduced in one or more dimensions. Their electromagnetic, mechanical, thermal, optical and chemical properties can be affected due to the size reduction. Quantum well (two-dimensional structures, 2D) is defined when only one length of a three-dimensional nanostructure is of a nanodimension; if two of the three-dimensional nanostructure is of nanodimensions while the other dimension remains large, then the structure is known as a quantum wire (one-dimensional structures, 1D). nanobelts and nanorods are also one dimensional structures. A quantum dot (zero-dimensional structure, 0D) is defined when three dimensions are in nano range. Nanoparticles are also regarded as zero-dimensional structure. Each structure of them has unique electronic structure. Figure 1.1 illustrates the processes of diminishing the size of a material.

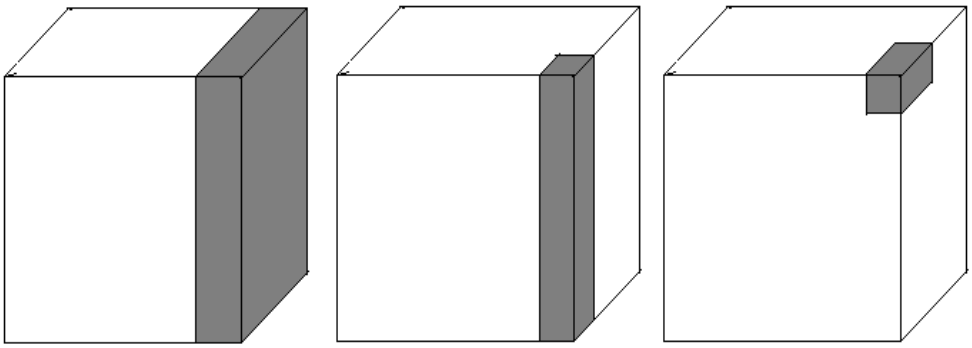

Figure 1.1: image (from left to right) of quantum well (shadow part), quantum wire (shadow part) and quantum dots (shadow part) compared to bulk material

A quantum well is a potential well that limits particles, which originally move free in three dimensions, to two dimensions, obliging them to occupy a planar region [3]. Due to its quasi-two dimensional (confined in z direction) natural, electrons in a quantum well have a density of states as a function of energy that has distinct steps while electrons in bulk material have a density of states that is a smooth, continue curve, as shown in Figure 1.2. Quantum well can be applied as a saturable absorber by taking advantage of its saturable absorption property. Saturable absorption defines as a property of materials when the absorption of light decreases with increasing light intensity. Saturable absorbers are widely used in mode locking lasers to assist in pulse duration, average powers, pulse energies and repetition rates.

In general, quantum wires have aspect ratios (length to width ratio) of 1000 or more. As electrons in quantum wires are quantum confined in two dimensions, they have

density of state which is quite different from that in bulk material and from that in quantum well. Quantum wires have unique properties such as the conductivity is much less than that of the corresponding bulk material for the wire width is much less than the free electron mean free path of the bulk material, and in this condition, scattering from the wire boundary will occur. The application of quantum wire is numerous. By now, quantum wires have been applied in building blocks for electronics, optics, mechanics and sensing technology etc. Quantum wires are widely used in sensor technology as quantum wires which are made of different material have different properties, for instance, Pd quantum wire is applied in H_2 gas sensor and it assist in quick responce time in room temperature operation surrounding; CH_4, NH_3, CO, NOx, O_2 gas sensors with the help of ZnO, SnO_2 or In_2O_3 quantum wires can have high sensitivity and work at room temperature; Ag quantum wires assist in explosive and drug sensors and they enable the sensors have fast response time, ultra sensitivity. Au quantum wires are mostly used in biosensors and detection of Mercury in water [4].

Quantum dots also exhibit quantum mechanical behaviours. Density of state of quantum dot is quite different from that of the bulk and that of 1D or 2D nanostructures as well. It is discrete other than gradual, only occupying certain permitted energy states. The property of quantum dots vary with the size of the quantum dots change. Larger quantum dots have a greater red spectrum shift compared to smaller ones and exhibit less pronounced quantum properties. Quantum dots can be used like a single-electron transistor in electronic applications. In addition, quantum dots technology is the most promising candidates in the application of solid-state quantum computation [5]. With the

help of quantum dots, the flow of electrons through the quantum dots can be controlled by only applying very small voltage to the leads, and spin can be precisely measured. Besides, quantum dots can also be applied in photovoltaic devices to increase the efficiency and reduce the cost.

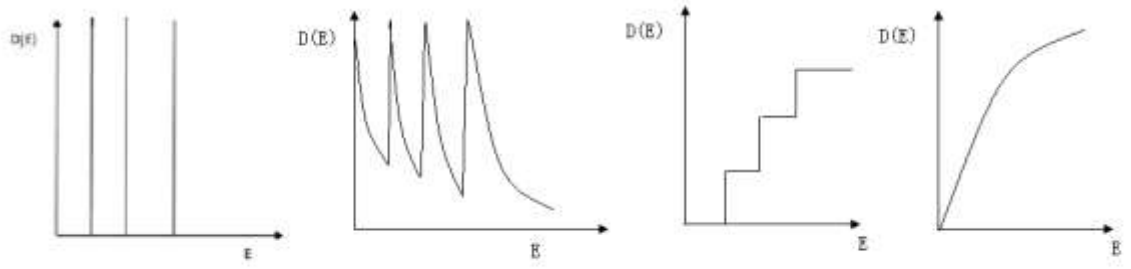

Figure1.2 : density of states of (from left to right) quantum dot; quantum wire; quantum well and bulk material [6]

Nanoparticles are defined as small objects which have the size between 1nm and 100nm. Nanoparticles are of great interest as they have different properties compared to the same material in bulk. Generally, a bulk material should have constant physical property while the property of nanoparticles is very size dependent. For example, bulk gold appears yellow in colour; however, it gradually changes its colour to red in liquid as metal gold is divided into tiny particles with the size less than 100nm. Colour is very size dependent because particles with different size will reflect light with different wavelength. Eventually, gold nanoparticles will turn invisible as they are too tiny to reflect any visible light. This is pretty useful in the application of cosmetic, packaging and coating.

Two of the major reasons to cause the differences in physical properties are

1) high increase in surface to volume ratio
2) the size of the particle moving into the area where quantum effects dominate

Surface to volume ration increases gradually as the particles are divided into smaller ones, and more surfaces mean more reaction areas. Atoms on the surface of a particle dominate the behaviour other than the interior atoms and this plays role in material isolation and interaction with others. Large surface area assists in making improvements in performance of fuel cells and batteries, in increasing strength and/or increasing chemical/heat resistance.

Methods to fabricate nanoparticles can be categorized into three:

1) vapour condensation
2) chemical synthesis condensation
3) solid-state condensation

Vapour condensation is applied in fabricating metal and metal oxide nanoparticles. It involves evaporation of solid metal followed by rapid condensation to form nano sized cluster. Inert gas is used during the procedure of fabricating metal nanoparticles as inert gas would avoid oxidation while oxygen is applied during the procedure of fabrication metal oxide nanoparticles. Temperature, evaporation rate, gas environment collectively determine final particle size. The main advantage of this technique is low contamination level [7].

Chemical synthesis, which require nanoparticles growing in the liquid environment which composed of plenty reactants, is the most widely used approach to product nanoparticles due to its low cost and high output. Chemical approaches are generally better than vapour condensation approaches for better controlling of the particle shape. Like vapour condensation, shape of the nanoparticles can be controlled by stopping the procedure when the desired size is reached; choosing a more stable chemicals and stopping growing at certain shape is another choice. However, contamination can be a problem need to be solved.

Solid-state approach creates nanoparticles by grinding and milling material. The milling material, milling time and atmosphere can affect nanoparticles together. Contamination is an issue in this approach as well.

1.3 Sensor and Biosensor (Nanotechnology Enabled Biosensor)

Sensors are devices that respond to some stimulus by generating a functionally related electrical signal. They convert a physical quantity, such as changes in ambient conditions, into a signal which can be observed by an observer or by an instrument. Measurement obtained by sensors can be used for some other purposes.

A sensor is supposed to be sensitive to the measurand and be insensitive to any other input quantities. Environmental effects such as temperature, humidity, shock and vibrations will affect the performance of a sensor in negative way; therefore, a strict transfer function is significantly necessary. Transfer function depicts the relationship between the input stimulus response and output electrical signal. Meanwhile, in general,

sensors should be inexpensive, reliable, and durable. Accurate, stable, high resolution, low cost sensing should be expected from a high quality sensor. No matter what special field a sensor would work in, all sensors should provide a great performance in accurate and stable monitoring of the measurand. Besides, dynamic range, response time, hysteresis, nonlinearity, noise and bandwidth are the important characteristics for sensors as well [8].

Sensor technology has been applied in physical, chemical and biological recognition systems. Sensors are used in household, environmental monitoring, medical diagnostics and health care and so on. Specifically, as an electrical devices, sensors can be used from surge protectors to automatic light switches, refrigerators and climate control appliances, toasters and in smoke and fire detectors. Aircrafts are embarked with sensors as they monitor position, wind speed, air pressure, and altitude and so on. For industry application, sensors constantly monitor to make the aim “maximize efficiency, minimize production cost and reduce waste” possible. In the field of health care and diagnostics, sensors can guide the biological systems running correctly and direct people to respond to the measurement, avoiding delayed reaction. In a word, sensors assist human being in contacting with the world.

A biosensor is a sensor which is stimulated by a biological element and proportionally converts the stimulus into an electronic signal. Biosensors consist of two parts, bioreceptor, and transducer. Figure1.3 depicts the components of a typical biosensor.

Bioreceptor is a biological recognition system and is capable of recognizing a specific target molecule. Transducer converts the interaction of analyte with the bioreceptor into a measureable, easily qualified value, such as electric signal. One point which is needed to notice is the bioreceptor is required to be immobilized intimately close to the transducer. Combined with the integrated circuit microchips technique, biosensors can be often referred as biochips. Generally, a biochip may consist of an array of individual biosensors and the biochip can be either used as an individual monitor or used for the analysis of multiple analyte [9].

Although biosensors are currently utilized in plenty of fields, developments are still required in the future generation of biosensors (Arntz et al. 2003):

1) The combination of a biologically sensitive part with a physical transducer for specific and quantitative detection of analytes
2) The ability of label-free detection of the biological interaction
3) The scalability of the sensors to allow massive parallelisation
4) Sensitivity of the detection range applicable for in vivo problems

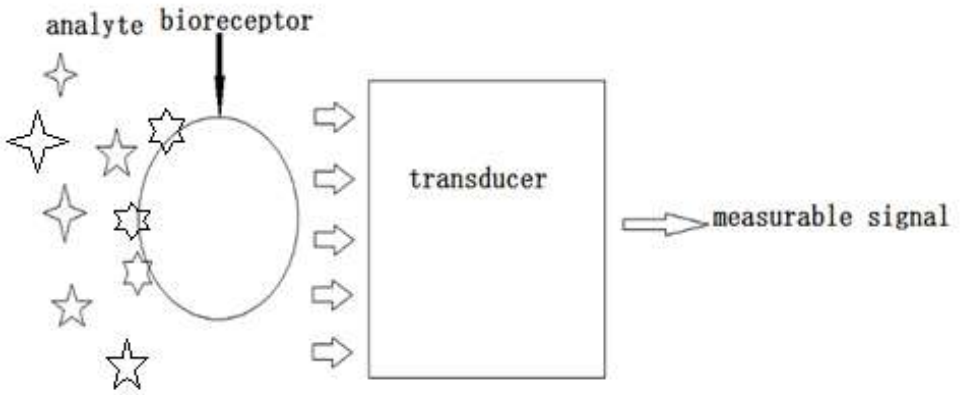

Figure1.3: components of a typical biosensor

Nanotechnology enabled biosensors have smaller size yet higher sensitivity and greater reliability. The most attracting reason is that sensitivity can be greatly improved for developing nanotechnology enabled sensors. Compared to conventional sensors which can only offer surface as sensing instrument, nanotechnology enabled sensors have the entire nanostructures can be affected by the analyte. As the size of nano-biosensor can be decreased down to a micrometer scale or even a nanometer scale, the sensitivity can be greatly increased; besides, nano scale structures provide the chance to observe new basic scientific phenomena that only occur when the dimensions are in small scale. A single molecule or atom can even be detected in potential when the sizes of the nanosensors go down to nanoscale. The small size, lightweight, and high surface to volume ratio of nanostructures contribute to break the previous limitation in sensitivity of conventional sensors, greatly increase the capability to detect chemical and biological species [6].

As mentioned above, sensors are supposed to insensitive to any other input quantities but the measurand. Therefore, selectivity is as important as the sensitivity, yet significantly more difficult to achieve. Frankly speaking, exclusively diminishing the size of the sensor to nano scale may not boost the selectivity, however, nanostructure materials and applying surface modifications and functionalization might work [6].

In addition, the responding speed with analyte can be absolutely affected by the size of the sensor. Compared to conventional sensors, nanotechnology enabled sensors have outstanding dynamic performance due to that nanostructures to assist in decreasing the time taken for a measurand to diffuse into and out of that volume. In nanostructures, the entire structure can be affected by the analyte, not only the surface [6].

Chapter 2: Theoretical background

2.1 Basic knowledge of Surface Plasmon Resonance (SPR) and Localized Surface Plasmon Resonance (LSPR)

The propagation of optical waves is generally evanescent, which means that the waves decay exponentially with distance from the point where they are propagated. However, some optical waves, as they oscillate perpendicularly to the direction of propagation, are transverse waves. An optical waveguide is defined as a path which limits optical waves within one or two dimensions.

The guided waves in a planar optical waveguide, which defines as a path that are only possible for certain propagation waves, are either TM (transverse magnetic or p-polarized) or TE (transverse electric of s-polarized) in two dimensions. Figure 2.1 shows the propagation of a transverse optical wave.

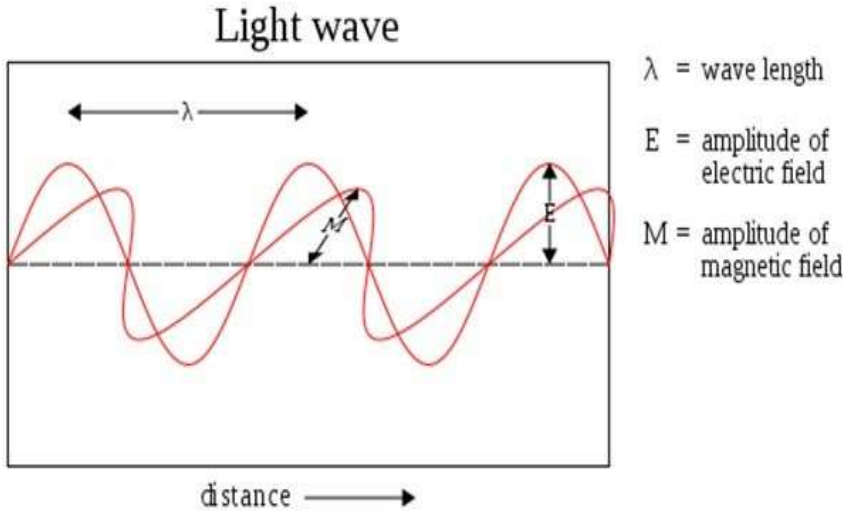

Figure 2.1: propagation of a transverse optical wave [10]

A Surface Plasmon is a charge density wave that exists at the flat smooth interface between a metal and a dielectric [11, 12]. Surface Plasmon (SP) is excited when waveguide thickness, d_f, decreases to a thin film of small thickness, as shown in Figure 2.2, then the waveguide changes to a boundary between the substrate and the sample media in surface. In addition, TM mode waves could be trapped near and around surface propagation along the boundary if waveguide is metallic [6].

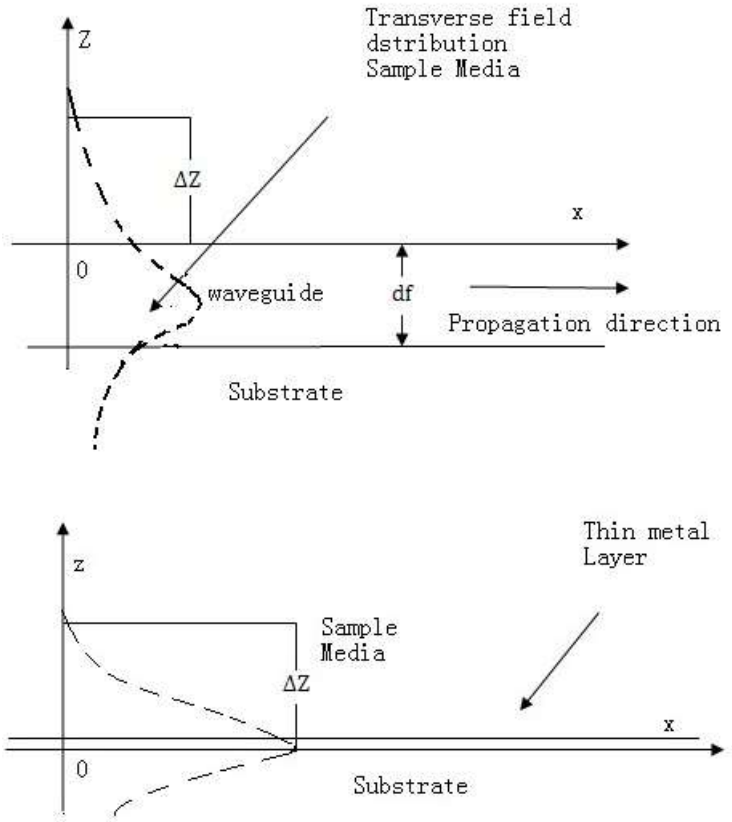

Figure2.2: (a) distribution of an evanescent wave in z direction; (b) A SP waveguide consisting of a thin metal film [6]

Penetration depth Δz, which is shown in the Figure 2.2, defines as:

$$\Delta z = \frac{\lambda}{2\pi}(N^2 - n_c{}^2)^{-\frac{1}{2}} \tag{2.1}$$

Where N, the effective refractive index, is an important parameter in sensing application as the sensors' sensitivity directly depends on it. n_c is the refractive index of sample media.

As SPs are coherent electron oscillations, the momentum and the energy of an incident photon must match that of a Plasmon for exciting SPs optically. Hence, light

energy can be effectively corresponding to a SP wave which results in strong absorption at certain wavelength and certain angle of incident light. One of two methods which are used to take SPR measurement is to measure absorption as a function of incident angle (also known as the angle method), and the other one is to measure absorption as a function of incident wavelength (also known as the spectral method). Proper wavelength and metal are chosen in the angle method while the precise incident angle, always within 0.0001^0, must be required in the spectral method [13].

Although SPR attracts great attention on monitoring biological interactions due to its non-invasiveness, free of dye labelling and producing results in real times, the stringent requirement of precise incident angle and wavelength control limits the development and application of SPR. Localized surface Plasmon resonance (LSPR), an unique optical property of noble metal nanoparticles, which exhibits a strong but narrow spectrally selective UV-visible absorption, relax the strict, severe requirement encountered in conventional SPR sensors. LSPR arises at specific wavelengths when the frequency of incident photon is resonant with the collective oscillation of the conduction electrons in the metal nanoparticles and it's very dependent on the size, shape, degree of particle-particle coupling of the nanoparticles, inter-particle spacing, and dielectric properties of the material, as well as the dielectric properties of the surrounding [14]. Along with the shape, size or some other related aspect of nanoparticles vary, the peak of the absorption band shifts. LSPR plays an important role in determining the magnitude of the enhancement factor in surface-enhanced Raman scattering and other surface-enhanced spectroscopy techniques. Therefore, a further understanding of unprecedented

levels of insight into these surface-enhancing properties can be done if only the LSPR of nanoparticles can be better understood and controlled.

Two optical parameters which are greatly controlled by the size and shape of the metal nanoparticles are the extinction wavelength (the wavelength of the maximum absorbance, λ_{max}) and the bandwidth. Take gold nanoparticles as an example, due to the extinction spectrum of gold nanoparticles is asymmetric, the bandwidth is defined as twice the difference between λ_{max} and λ which is at half-maximum on the higher wavelength side of λ_{max}. In general, increase of the nanoparticles size will results in the peak of the absorption shifting to longer wavelength (red shift) and broadening in bandwidth. This phenomenon is mainly attributed to the phase-retardation effects in larger nanoparticles [15, 16] and contribution of scattering to the extinction. Besides, the extinction intensity is also controlled by the contribution of scattering to the extinction spectrum [17].

Extinction, E (λ), which equals to the sum of absorption and Rayleigh scattering, can be measured by UV-visible extinction spectroscopy and defines as:

$$E(\lambda) = \frac{24\pi N_A a^3 \varepsilon_m^{\frac{3}{2}}}{\lambda \ln 10}\left[\frac{\varepsilon_i}{(\varepsilon_r + 2\varepsilon_m)^2 + \varepsilon_i^2}\right] \quad (2.2)$$

Where N_A is the area density of nanoparticles, a is the radius of the metallic Nanosphere, ε_m is the dielectric constant of the medium around the metallic nanoparticles, ε_r and ε_i are the real part and imaginary part of the metallic nanosphere's dielectric function respectively, and λ is the wavelength of the absorbing radiation. LSPR

condition can be achieved when the term $(\varepsilon_r+2\ \varepsilon_m)^{\ 2}$ equals to zero. According to Equation (2), LSPR spectrum is very dependent on the nanoparticles radius a, the nanoparticles material (ε_i and ε_r) and the surrounding dielectric constant (ε_m).

However, as in the real case, nanoparticles are generally not spherical; the extinction spectrum is affected by the in-plane diameter, out-of-plane height and shape of the nanoparticles; and meanwhile, the $(\varepsilon_r + 2\varepsilon_m)$ term will be replaced by $\varepsilon_r+\chi\ \varepsilon_m$. Here, χ is a shape factor term which describes the aspect ratio of nanoparticles. The values of χ ranges from 2 (for a sphere) up to, even beyond value of 17 for 5:1 aspect ratio nanoparticles [18]. In addition, the LSPR is affected by interparticle spacing and the substrate dielectric constant as well.

Therefore, the extinction maximum (λ_{max}) of nanoparticles will shift when the local environment already changes. This phenomenon is the basis of a sensor to detect. The shift in extinction maximum can be calculated

$$\Delta\lambda = \lambda_2 - \lambda_1 = m\Delta n[1 - e^{-\frac{2d}{I_d}}] \qquad (2.3)$$

Where, λ_2, and λ_1 are the maximum absorption wavelength with and without specimen. m is the bulk refractive-index response of the nanoparticles, Δn is the change in refractive index; d is the effective thickness of the adsorbate layer and I_d is the characteristic electromagnetic-field-decay length, which is called decay length for short after. Decay length is a function of excitation wavelength.

Refractive index of the surrounding environment could be varied by exposing the nanoparticles to different solvents. In addition, similar wavelength shifts can be also observed when molecules bind to the nanoparticles surface and result in the change of the surrounding local refractive index while leaving the bulk refractive index essentially unchanged. For the case of biosensors, biomolecules such as DNA and protein have been studied by taking advantage of LSPR. LSPR resonant wavelength will shifts towards the longer wavelength region once the biological targets attach to the surface of the nanoparticles structure. Meanwhile, the coverage of the target analytes binding on the nanoparticles structure surface will determine the magnitude of the LSPR shift response.

2.2 Comparison between Optical Transduction Based on SPR and LSPR

Surface Plasmon Resonance (SPR) sensors detect the local refractive index changes that occur when the target analyte binds to the metal film and have been widely used to monitor a broad range of analyte-surface binding interactions including the adsorption of small molecules [19], ligand-receptor binding [20], and protein adsorption on self-assembled monolayer [21], antibody-antigen binding [22], DNA and RNA hybridisation [23].

Localized Surface Plasmon Resonance (LSPR) nanosensors retain series of advantages, such as high selectivity, label-free operation, capability to probe complex mixtures without purification and multiple detection modes (extinction and resonance Raylengh scattering) to sensors based on SPR spectroscopy, besides, LSPR based

nanosensors exhibit unique properties such as faster response times, smaller pixel size, higher spatial resolution and simultaneous surface-enhanced RAMAN scattering. Comparison between SPR and LSPR based nanosensors are listed in detail in Table 2.1 [18].

According to the Table 2.1, SPR based nanosensors seem exhibiting larger refractive index sensitivity, in which 2×10^{6}nm/refractive index unit (RIU) can be obtained while only maximum 2×10^{2}nm/RIU can be obtained for LSPR based nanosensors. A result the LSPR based nanosensors were regarded 10,000 times less sensitive than the traditional SPR nanosensors, nevertheless, the short and tuneable characteristic electromagnetic field decay length can help LSPR based nanosensors having a competitive performance as SPR nanosensors.

Table 2.1: Comparison between SPR and LSPR based sensors [18]

Instrument characteristic	SPR	LSPR
Label-free detection	Yes	Yes
Distance dependence	Around 1000nm	30nm(size adjustable)
Refractive index sensitivity	2×10^{6} nm/RIU	2×10^{2} nm/RIU
Modes	Angle shift Wavelength shift Imaging	Extinction Scattering Imaging
Temperature control requirement	Yes	No
Chemical identification	SPR-Raman	LSPR-SERS(surface-enhanced Raman scattering)
Field portability	No	Yes
Commercially available	Ye	No
Cost	Ranging from $150,000 to $300,000	$5000 (multiple particles) $50,000(single nanoparticle)
Spatial resolution	Around 10×10μm	Nanoparticles
Nonspecific binding	Minimal (determined by surface chemistry and rinsing)	Minimal (determined by surface chemistry and rinsing)
Real-time detection	Time scale=10^{-1}-10^{-3}s,planar diffusion	Time scale=10^{-1}-10^{-3}s,radial diffusion
Multiplexed capabilities	Yes	Yes-possible
Small molecule sensitivity	Good	Better
Microfluidics compatibility	Yes	Possible

In the case of SPR based nanosensors, the decay length I_d is 15~25% of the light's wavelength. On the other hand, the decay length of LSPR based nanosensor is around 1~3% of the light's wavelength and it depends on the size, shape, composition of the nanoparticles as well [18]. LSPR benefits in its small decay length, which represent a short range electromagnetic field enhancement, due to the fact that fields can be highly localized and confined to small volumes around the nanoparticles.

Also, the smallest footprint of the SPR and LSPR sensors are different. In practice, SPR sensors require at least a 10×10um area for sensing experiments while for LSPR sensing, the footprint size can be reduced down to a single nanoparticles (with the in-plane width of around 20nm) by using single nanoparticles measurement techniques [24].

In addition, high refractive index means that SPR based nanosensors are required to control the working temperature as the temperature change induces the change in refractive index, while LSPR are less sensitive to the temperature changes.

Finally, as the table 2.1 clearly describes, the cost of commercialised SPR instruments is between $150 000 and $300 000 whereas the cost for a LSPR system is less than $5 000.

2.3 Nanosphere lithography

As it was described above, the wavelength corresponding to the extinction maximum, λ_{max} of the LSPR is very dependent on the size, shape, interparticle spacing, and wavelength-dependent dielectric constants of the material from which the nanoparticles are composed [18]. Size-dependent properties of interest include optical [25], near field scanning optical microscopy [26], surface-enhanced spectroscopes [27], and chemical and biological sensors [28, 29].

Generally, two complementary approaches, bottom-up approach and top-down approach are used for the creation of nano-structured materials. Top-down approach depicts those material in bulk are deduced into nanometer scale. By using this technique, cluster structure, number of surface vs. interior atoms and quantum confinement effects play roles in controlling the size-dependent properties. Top- down approaches use advanced lithographic technologies to reduce the dimensions of bulk matter form the um to the 10 nm scale. Lithographic techniques, such as photolithography, electron beam lithography (EBL), X-ray lithography (XRL), and ion beam lithography (IBL) are generally used to create surface nanostructures with controlled size, shape and interparticles spacing [30].

Photolithography technique is the most widely used to fabricate microstructure however, due to its limit of diffraction resolution EBL, IBL, and XRL techniques are used mostly to fabricate nano-structure. However, all these techniques have inherent shortages that limit their applicability in many conventional laboratory situations. Both

EBL and IBL have low sample throughput and high cost per nanostructure. XRL, though offset its high capital cost by its high throughput, still experiences limitation due to problems with photoresist development, mask proximity and a small feature size limit in the 20-30 nm range caused by photoelectron generation in the mask an diffraction effects [30].

On the contrast, nanosphere lithography (NSL) technique is an inexpensive (less than 1$ per sample), with high-throughput. NSL is an ideal fabrication tool to produce regular, periodic, almost homogeneous arrays of nanoparticles with tunable shapes, sizes, and interparticle spacing, d_{ip}, by selecting an appropriate nanosphere diameter, D, and deposition mass thickness, d_m. The diameter of the in-plane particle d can be described as the following equation:

$$d = \frac{3}{2}\left(\sqrt{3} - 1 - \frac{1}{\sqrt{3}}\right)D = 0.233D \qquad (2.4)$$

Where, D is the diameter of the polystyrene sphere. Generally, NSL involves a process that a suspension of polystyrene nanospheres of size-monodisperse self-assembles into a crystalline monolayer with the help of surfactant. Methods for smooth deposition of a suspension onto a substrate include spin coating, drop coating, and thermoelectrically-cooled angle coating. All of these deposition methods demand the nanospheres being capable to diffuse freely across the substrates to seek the lowest energy configuration. The prosperous of the most basic NSL architecture and many new nanostructure derivatives are mainly due to the need for monodisperse and reproducible. Dr. Richard P. Van Duyne et al. created nanosphere lithography monolayer by spin-coating polystyrene

nanospheres. Nanospheres with different sized were spin-coated at different speed [30]. Dr. John R. Dutcher et al. created their monolayer on both hydrophilic and hydrophobic substrates by convective self- assembly. They spread a drop of suspension with a given volume over the accessible glass area encircled by a Teflon ring [31]. Dr. Simona Badilescu et al. immersed the substrate into the burette containing a mixture of the PS spheres and Au colloids. By controlling the flow rate of the suspension, well- ordered film can be found in the lower part of the substrate [32].

2.3.1 Basic knowledge of self assembly

Self assembly is a process in which atoms, molecules, nano-particles and other building blocks attach to functional systems in an ordered manner and is generally self-driven by the energies of such systems [33]. Self assembly involves series of reactions which consist of place or deposit material that forms an island on substrate. Those atoms or molecules of the material either are adsorbed and diffuse freely on the surface until they join or nucleate with another adsorbed atom to form an island, attach themselves to or aggregate into an existing island, or desorbed and therefore leave the surface. Small islands can maintain growing, migrate to other places, or evaporate [34]. Gibbs free-energy determinately affects the island formation process. Gibbs free energy defines as an available free energy in a spontaneous chemical reaction within a system; the change of the Gibbs free energy contributes to keep the system being more thermodynamically stable. Overall Gibbs free-energy density g can be depicts as following:

$$g = (1 - \varepsilon)g_{sur-vac} + \varepsilon(g_{sur-lay} + g_{lay-vac}) \quad (2.5)$$

where ε is the covered fraction of the surface and $g_{sur-vac}$ is the Gibbs free-energy density between the bare surface and the outside vacuum or surrounding, $g_{sur-lay}$ is the Gibbs free-energy density between the surface and the layers of adsorbed atoms, the $g_{lay-vac}$, is the free-energy between these layers and the vacuum.

Relative contributions among these free-energy densities gradually change along with islands form and grow, and the growth process evolves to maintain the lowest thermodynamic free energy. Spreading pressure P_s is defined as the difference between the bare surface free energy density ($g_{sur-vac}$) and layers free energy density ($g_{sur-lay} + g_{lay-vac}$), which means,

$$P_s = g_{sur-vac} - (g_{sur-lay} + g_{lay-vac}) \quad (2.6)$$

In this case, Eq. (2.5) can be rewritten as

$$g = g_{sur-vac} - [g_{sur-vac} - (g_{sur-lay} + g_{lay-vac})]\varepsilon$$

$$= g_{sur-vac} - P_s \times \varepsilon \quad (2.7)$$

For the condition $g_{sur-vac} > (g_{sur-lay} + g_{lay-vac})$, which means a spreading pressure P_s is positive, ε increases to decrease the overall free energy. In this case, the adsorbed atoms will tend to remain directly attaching on the blank surface, growing in horizontal direction, and eventual forming monolayer. This is known as the Franck-van der Merwe growth mode. On the contrary, for the condition $g_{sur-vac} < (g_{sur-lay} + g_{lay-vac})$, which means the spreading pressure P_s is negative, free energy maintains low value by decreasing ε

and eventually causes newly added adsorbed atoms to aggregate on the top of existing islands for decreasing the free energy. This is known as Volmer-Weber mode of growth [34]. Figure 2.3 shows the mode of the thin film formation.

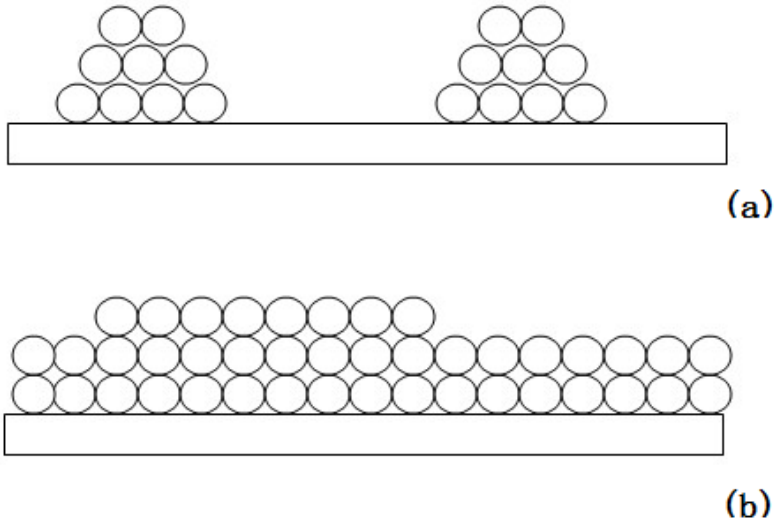

Figure 2.3: the modes of the formation of the thin film. a) is Volmer Weber (island growth) mode and b) is Frank-Van der Merwe (layered growth) mode

The ordered 2D array of a monolayer is the nanostructure which was utilised in this research. The ordered 2D arrays of nanostructures are applied in a number of areas such as antireflection coatings, regular arrays of microelectrodes, and selective solar absorbers; to function as active layers to enhance Raman scattering or to improve

photovoltaic, to work as supports in biosensing or heterogeneous catalysis and to perform as arrays of quantum dots or single-electron transistors.

Those monodispersed colloidal spheres can be self-assembled into ordered 2D arrays on solid supports or in thin films of liquids usually using three methods. The first method is to form a 2D array of colloidal spheres at the air-liquid interface and this array can be transferred onto the surface of a solid substrate; the second method is usually referred to as electrophoretic deposition [35]. In this method, a liquid dispersion of colloidal spheres is confined between two parallel solid electrodes. The colloidal spheres which initially deposit randomly on the anode will move toward each other to form a stable 2D hexagonal array structure when a sufficiently strong electric field is applied.

In this research, 2D array of polystyrene is formed in terms of the third method, which takes advantage of the capillary forces. Capillary forces result in the capillary action which is a phenomenon where liquid will automatically rise to a higher lever within a capillary tube than the water outside. The capillary tube, which is immersed in water vertically with both ends open, is as small as a hair [36]. Besides capillary tubes, capillary action also occurs in porous material, such as tissue, and non-porous material, for example, liquefied carbon fibre. The attractive capillary forces among colloidal spheres organize them into a hexagonal 2D array in a thin film of liquid supported on a flat substrate. A liquid dispersion of colloid spheres is required to be well spread onto the surface of a solid substrate. As the solvent evaporates, the capillary force will draws the nanoparticles together into hexagonal closed-packed form. Nagayama and co-workers followed this self-assembly process experimentally by using an optical microscope [37].

They found that a well ordered nucleus, which consists of a number of colloidal spheres, was first formed when the thickness of the liquid layer approached the diameter of the colloids. More colloids were driven toward this nucleus by a convective transport and eventually organized around the nucleus due to the attractive capillary forces. A flat, clean and chemically homogeneous surface has to be used in order to generate a highly ordered array with relatively large domain sizes.

However, impurities are inevitable during the formation of the monolayer. Similar to those defects which are found in any crystal, missing nanospheres (vacancies), site randomness, slip dislocations (line defects) and polydispersity, multilayer domains are the main defects in NSL.

There is no tight, efficient control over the density of defects and the size of domains during the process of self-assembly. However, the defect-free area of monolayer which is formed through NSL typically ranges from 10μm to 100μm [38].

Monolayer of nanospheres acts as a deposition mask through which the metal is deposited. After removing the monolayer, an array of ordered, uniformed and size-controlled metal nanoparticles will be left behind. Beside, size and height of nanoparticles can be tunable by varying the size of the polystyrene and the amount of deposition metal respectively. Consequently, NSL is capable of producing well-ordered, 2D periodic arrays of nanoparticles from a wide variety of materials on several substrates.

Chapter 3: Fabrication Facilities, Characterization Methods and Measurements

The major facilities are used to fabricate and characterize the devices are described in the following sections:

3.1 Sputtering technique

Sputtering technique is used to obtain materials thin film deposition. In sputtering technique, solid material is bombarded with energetic ions to create a cascade of collisions in the target material's surface. Atoms which are ejected by those multiple collisions are directed towards the target substrate in gas phase to form a thin film. The number of atoms ejected from the surface per incident ion is called the sputter yield and the ions for the sputtering process are produced by plasma which is generated above the target material. The atoms sputtered from the surface of the target enter the plasma where they are excited and emit photons [6].

A traditional diode plasma (or DC sputterer) is simply a diode which includes an anode and a cathode inside a vacuum system, shown as Figure3.1.

Applying certain voltage across the electrodes and a suitable gas pressure, the gas breaks down into plasma. Inert gas, such as argon, is applied during the sputtering procedure to ensure the composition of the deposited thin film is exactly the same as the target material. Metal oxide thin film can be produced by introducing oxide gas into the

vacuum chamber because the chemical reaction between the target material and oxide gas can result in the reactive sputtering processes.

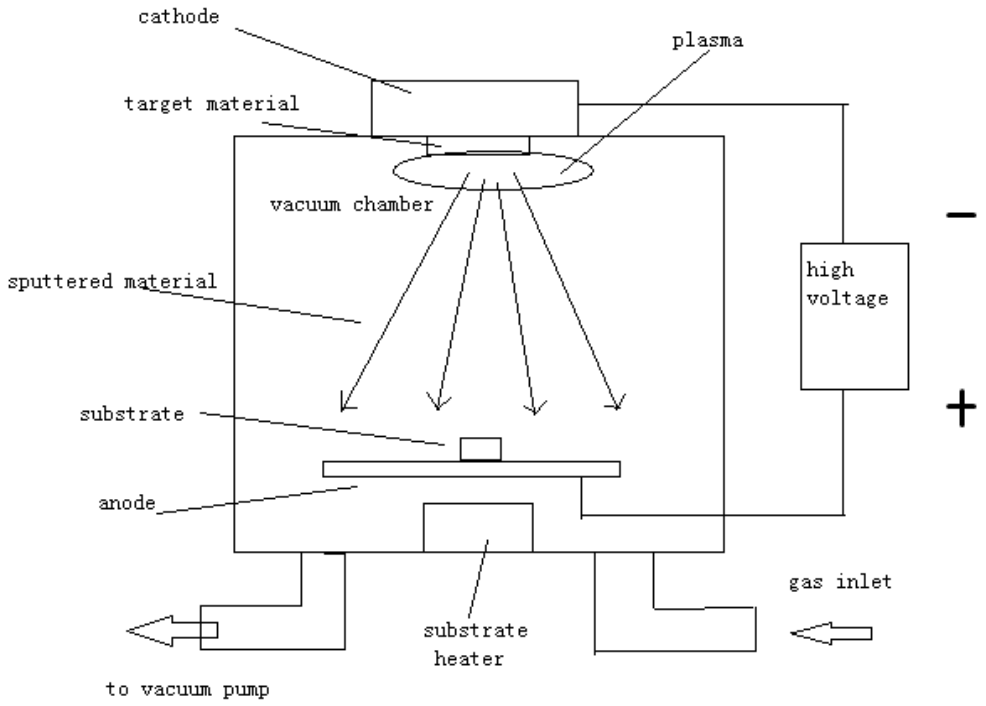

Figure 3.1: a diagram of a simple diode sputtering system [6]

Deposition rate can be varied by changing the distance between the target and the substrate, the power applied and the energy applied to the target, and it depends on the softness of the target as well. Meanwhile, deposition rate, inside temperature can also affect the shape of the deposited materials thin films.

The following major instruments were used to fabricate, observe and characterize the prepared samples, and devices discussed in this research.

3.2 Scanning Electron Microscopy (SEM)

The SEM might be the most routinely utilized instruments for the characterization of nanomaterials. It scans a sample with a beam of electrons that interact with the sample to obtain secondary electron images of organic and inorganic materials with nanoscale resolution and get the topographical and morphological information [6].

A typical schematic diagram of an SEM is shown in Figure3.2. The electron beam is emitted from a heated filament which is usually made form lanthanum hexaboride (LaB_6) or tungsten. Certain voltage is applied on the filament to induced electrons to be emitted. The electron beam is focused by a condenser lens then followed by an objective lens and raster-scanned over the sample by scanning coils [6].

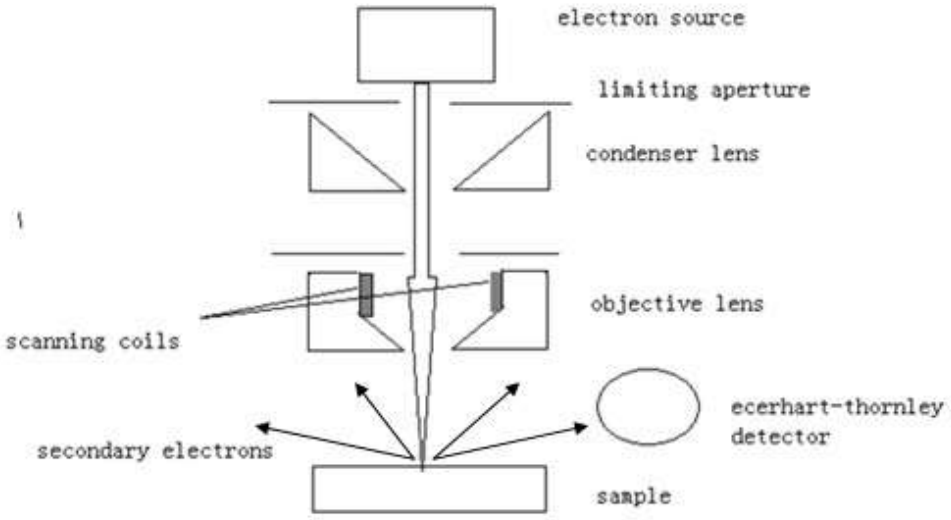

Figure 3.2: a typical schematic diagram of an SEM [6]

When the primary electron beam hits the sample, secondary electrons emission occurs as part of the primary electron beam energy will be absorbed by the electrons in the sample. The secondary electrons, which have lower energies, are collected by an Everhart-Thornley detector, converted to a voltage, amplified and eventually build the image. The intensity of the secondary electrons is displayed through the position of the primary bean on the sample. Meanwhile, the samples which can be placed in the SEM are required either conducting or covered with a thin metal layer for avoid electric charging. In addition, scanning at low pressures can also ensure the electrons are not scattered by gas molecules inside the chamber [6].

3.3 UV-Vis spectrophotometer

Ultraviolet-visible (UV-Vis) spectrophotometer is widely utilized to quantitatively characterize organic and inorganic nanosized molecules, besides; it is used for sensing applications as well. The samples may exist in gaseous, liquid or solid form. Different sized materials, which range from transition metal ions and small molecular weight organic molecules to polymers, nano-particles, can be characterized. Size dependant properties of nano scaled particles can also be observed in a UV-visible spectrum by measuring the peak broadening and shifts in the absorption wavelength [6].

Spectrophotometers are categorized as two major classes: 1) single beam and 2) double beam. A single beam spectrophotometer measures the intensity of the absolute light and a double beam spectrophotometer measures the ratio of the light intensity on

two different light paths. Basically, double beam technique can provide easier and more stable measurement while single beam technique can have a larger dynamic range.

A spectrophotometer consists of a spectrometer which produces light of any selected color (wavelength) and a photometer, which measures the intensity of light. Most organic and inorganic compounds show specific absorption bands due to the fact that the UV-Vis spectra originate from the electronic transitions in molecules. Prior to the measurement of the absorption band, auto zero should be calibrated to set the absorption of some standard substance as a baseline value. In this condition, the absorption of all other substances are measured relative to the initial zero substance.

For a monochromatic light, a quantitative relationship between the intensity of the transmitted light and the concentration of the colored compound is given by equation 3.1

$$I = I_0 \times 10^{-KCL} \tag{3.1}$$

Where I is the intensity of the light transmitted through the sample, I_0 is the intensity of transmitted light using the pure solvent, C is concentration of the colored compound, L is the distance of the light passes through the solution and K is a constant.

Given the light path L is a constant as it is fixed in the spectrophotometer, Equation 3.1 can be written as:

$$I/I_0 = 10^{-K'C} = T \tag{3.2}$$

Where K' is a new constant and T is the transmittance of the solution.

Equation 3.2 can also be written in a logarithmic manner:

$$-\log T = \log {}^{1}/_{T} = KC = \textbf{Optical density} = \textbf{absorbance} \quad (3.3)$$

Equation 3.3 clearly depicts the relationship between transmittance and the concentration of the colored compound. The absorbance is directly proportional to the concentration of the colored compound.

Beside the colored compound that can be measured by the spectrophotometer, most organic and inorganic compounds also show specific absorption bands because the UV-Vis spectra originate from the electronic transitions in molecules. The main processes in the spectrophotometer are

1) the light source passes through the sample
2) the sample absorbs light
3) the detector detects how much light the sample has absorbed
4) the detector then converts how much light the sample absorbed into a number.

3.4 Atomic Force Microscope

Atomic Force Microscope (AFM) has the function of measuring attractive or repulsive forces between the scanning probe tip and the sample surface and obtaining the surface image in atomic-scale.

When the distance between AFM tip and the sample surface is as close as several nanometers, forces between atoms in the tip and in the sample will trigger tip deflection. Those forces, such as Van der Waals, electrostatic, magnetic, capillary, Casimir, and salvation forces, can be measured through the amount of the deflection. AFM is not only applied in measuring forces or obtaining surface topography, it is also used as a current, chemical, physical and biosensor. [39, 40, 41, 42]

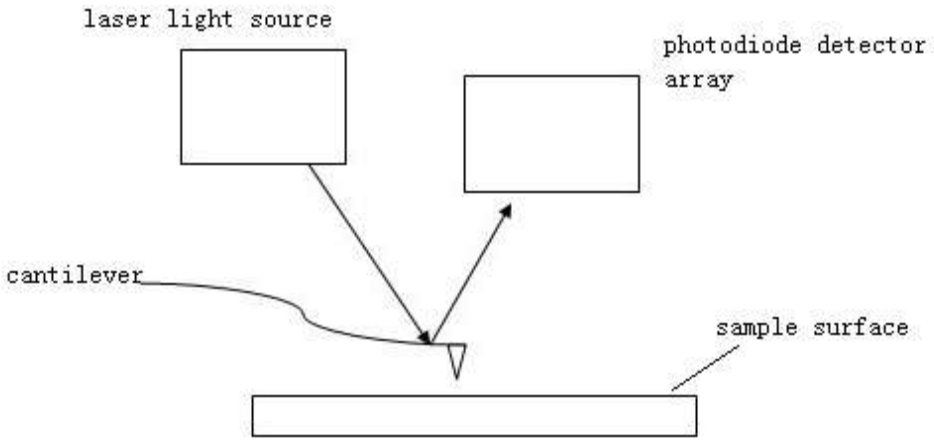

Figure 3.3 a typical configuration of AFM

The AFM has a microscale cantilever which is made from silicon or silicon nitride; laser light which is emitted from the laser light source reflect onto a position sensitive detector which is made from an array of photodiodes. Figure 3.3 shows a simple AFM setup. The curvature radius of the sharp tip which locates at one end of the cantilever is around nanometers. Forces act between the sharp tip and the sample surface

when the two parts are close enough and result in that cantilever bends and deflects in a similar manner to a tiny diving board. The forces will be indirectly calculated by measuring the deflection of cantilever. According to Hooke's law, forces can be calculated by the following equation:

$$F = -kz \tag{3.4}$$

where F is the force, k is the stiffness of the cantilever and z is the distance which the cantilever bents. Samples are immobile on a piezoelectric stage whose position can be accurately determined by applying a voltage, thus, the cantilever's deflection is measured by the variation of the position. Usually, the approach to measure the cantilever deflection is to measure the variation of the laser light's reflection position on the photodiode detector.

Several operation modes exist, contact mode, constant force mode and dynamic force mode (tapping mode). Among these approaches, contact mode, where the tip is directly contact with the surface, is the most common one. Another method is constant force mode where the tip maintains a constant height above the surface. Dynamic force mode requires a stiff cantilever oscillates within close proximity of the surface. Changes, which is result from that part of the tip occasionally touch or tap the surface during the oscillation, in the resonant frequency or amplitude of the cantilever are measure during a scan.

Chapter 4: Device Fabrication

In this research we have fabricated several samples/devices on glass and single crystalline silicon substrates. In the following sections we first discuss the samples preparation then we describe techniques and methods used to fabricate the final devices.

4.1 Substrate preparation

Rectangular glass substrates (with dimensions of 7 x 0.8 x 0.1 cm) as well as pieces of single crystalline silicon wafers used in this research work were prepared as follow:

1) Glass substrates were first washed with soap and abundant of water

2) Substrate were fully rinsed by de-ionized water and acetone

3) Then isopropanol was used to remove acetone and degrease the substrates

4) Substrates dried by nitrogen gun at room temperature

5) While the samples were drying, solution of 3-Aminopropyltriethoxysilane (APTES) in acetone (1% in volume) was prepared

6) Then the samples were immersed in this solution away from direct light for 24 hours

7) The substrates then were washed by acetone and isopropanol again, and then repeat step 4

The amount of water is significant in the process of silanization. An overabundance of water will cause excessive polymerization in the solvent phase, and the easily formed silane multilayers are supposed to be avoided as they will cause aggregation of metal nanoparticles during chemisorptions on the surface (the aggregated metal nanoparticles will cause an increased absorbance at higher wavelengths) [17]. On the other hand, a deficiency of water will attribute to the formation of an incomplete monolayer [43]. APTES is widely used to make metal nanoparticles attached to silica substrates due to the strong interaction between the amine group and the metal particles [44, 45]. APTES is attached to the substrate because of the hydrolysis, which attributes to siloxane bonds at the substrate surface. Besides, compared to the non-aminated silane, amines function in APTES will self-catalyze the hydrolysis reaction, which is propitious to form monolayer. However, silanization time must be critically controlled as over silanization will result in the roughness of the substrates surface.

Silane molecule with amino (NH_2) group is shown in Figure 4.1. The long pair of the nitrogen atom will assist in adherence between metal nanoparticles and glass substrate.

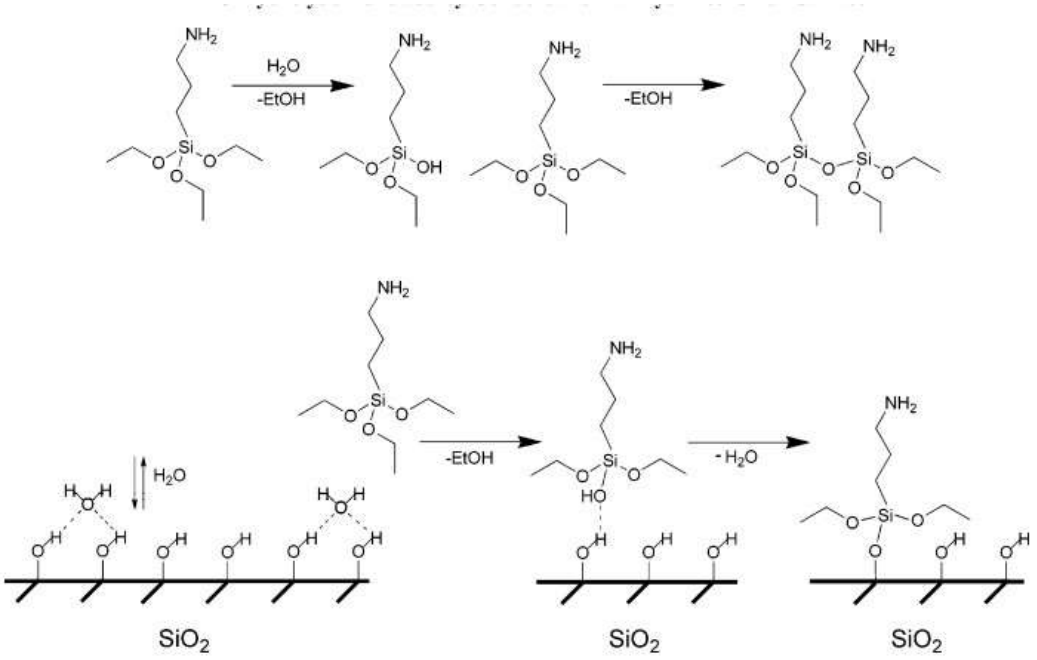

Figure 4.1: Top figure of APTES Hydrolysis is followed by Condensation Reaction in Solution Phase. Bottom figure of APTES Hydrolysis is followed by Condensation at Hydrated Silica Surface [46].

Likewise glass substrate, pieces of silicon wafers were prepared as the following steps:

1) Silicon wafers were rinsed with de-ionized water.

2) Rinsed in acetone.

4.2 Silver Colloids Nanoparticles and Polystyrene Particles Preparation

Three methods were used to obtain silver colloids in this research. Silver nitrate solution was used in all these methods and different chemicals were added to reduce the silver colloids in each approach. These chemical were:

1) Sodium citrate, $C_6H_5O_7Na_3$

2) Hydroxylamine hydrochloride, NH2OH.HCL and Sodium hydroxide, NaOH

3) Sodium citrate, $C_6H_5O_7Na_3$ and Borohydride, $NaBH_4$.

I. Sodium Citrate method

In this method, noble metal colloids were prepared with sodium citrate solution ($C_6H_5O_7Na_3$) and silver nitrate ($AgNO_3$) solution. The following steps were followed to prepare the solution.

1) Dissolve 0.017g $AgNO_3$ in 100ml de-ionized (10^{-3}M) water.

2) Heat the solution until to boil.

3) Add 2 ml of 1% sodium citrate solution, drop by drop

4) Keep heating for 10 minutes, until the solution color changes to grey green.

At first, the solution would turn into yellow and gradually into dark orange, eventually the color would turn into grey green. Silver colloids with sizes of 30 -40 nm were produced in this way. Substrates were immersed into the solution and left in an oven, keeping the temperature in range of 50~60 degree. Substrates were taken out once the solution was completely dried.

II. Hydroxylamine hydrochloride method

In this method, Hydroxylamine hydrochloride and Sodium hydroxide were added to the silver nitrate solution. The steps were as followed:

1) Dissolve 0.017g $AgNo_3$ in 100ml de-ionized (10^{-3}M) water.

2) 0.021gm of $NH_2OH.HCL$ is dissolved in 5 ml DI water

3) Add 4.5ml NaOH solution (0.1M) to $NH_2OH.HCL$ solution

4) Rapidly add the prepared mixed solution which was prepared in step 3 to the silver nitrate solution

The solution turned to grey-brown in a few second.

III. Borohydride method

In the last method, both Sodium citrate solution and Borohydride solution were used in the following procedure:

1) Add 1 mL of 1% Silver nitrate to 100 mL DI water

2) Add 1mL of 1%(w/v) sodium citrate into the solution prepared above

3) Wait for 1 min.

4) Then 0.075% $NaBH_4$ in 1% sodium citrate was added

The solution changed its color into dark green immediately. The size of the silver colloid was 21±9nm [47].

In this research, the silver colloids which were prepared with Sodium Citrate method (method I) were eventually used during the deposition of metal nanoparticles.

Besides for the preparation of silver colloid, polystyrene (PS) suspension in water with average diameter of 420nm and 920nm (5% by volume) were diluted to 1% suspension. Meanwhile, surfactant (0.2% n-dodecyl-sodium-sulfate) was prepared in the research, for assisting polystyrene suspension in well spreading and wetting the substrates.

4.3 Polystyrene template preparation using Self Assembly Technique

Self-assembled monolayer takes advantage of the self-assembly process. The polystyrenes start with clusters and then form themselves into a layer on the substrate by themselves. The polystyrenes either form monolayer or multilayer for maintaining the lowest thermodynamic free energy. Therefore, concentration of the polystyrene suspension and the deposition method should be precisely chosen. In our research, we describe a simply and convenient method based on nanosphere lithography to fabricate monolayer.

4.3.1 Polystyrene Template self assemble on Silicon Substrate

At the very beginning of the research, silicon substrate was placed horizontally on a table. One drop of the polystyrene suspension (1%) with the diameter of 420nm was dropped on the silicon substrates and followed by one drop of surfactant. Mix and spread the solution well and use a syringe to remove the excess solution. Substrates were dried at room temperature for about 10 minutes, and polystyrenes were self assembled. The image of the layer is shown in Fig 4.2. As the figure shows, silicon substrate is a good choice to produce monolayer.

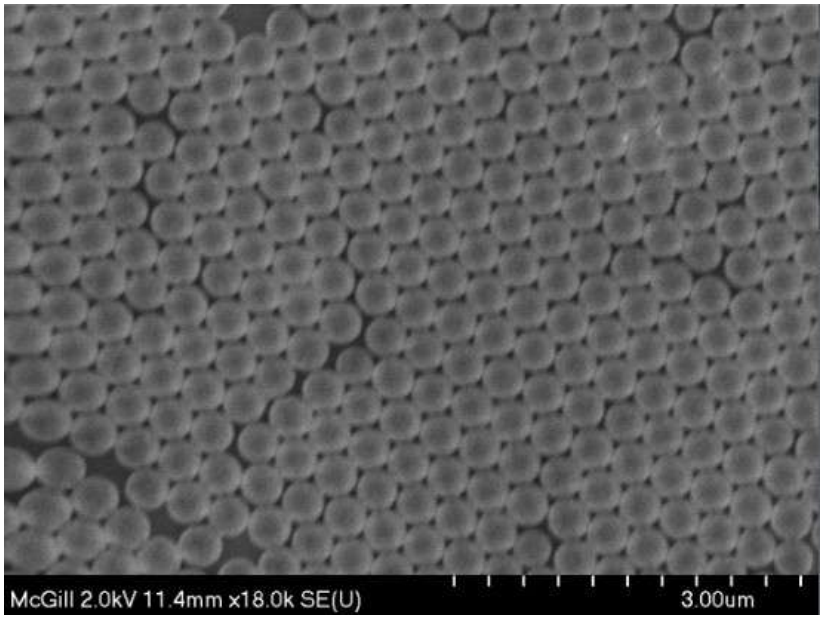

Figure 4.2: SEM image of monolayer which was prepared by 420nm polystyrene on silicon substrate

4.3.2 Polystyrene Template self assemble on Glass Substrate

The same procedure was done on glass substrate as what had done on silicon substrate in Chapter 4.3.1. However, the polystyrenes suspension with the same concentration forms differently on different substrate, as shown in Figure 4.2 and Figure 4.3. For silicon substrate, it is easy to get well-ordered uniform monolayer, as it is shown in Figure 4.2, while it is quite severe situation for glass substrate as polystyrenes form as polymers, and the image is shown as Figure 4.3.

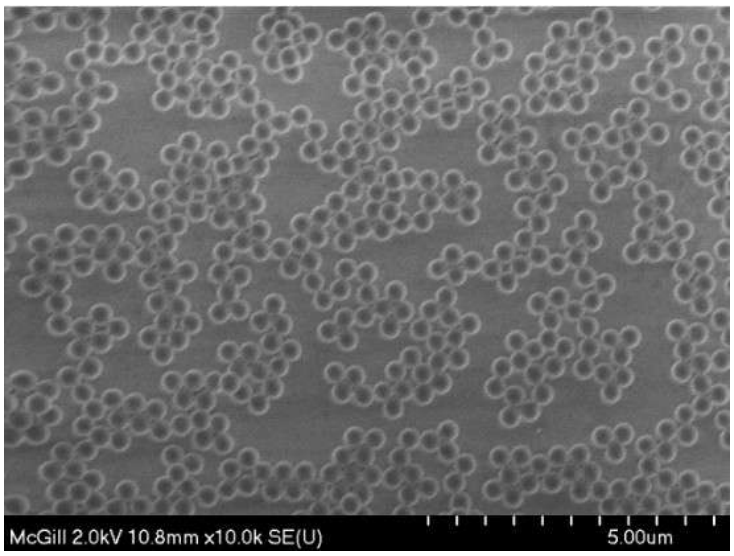

Fig4.3 SEM image of polymer which prepared by 420nm polystyrene on glass substrate

Fortunately, given that a very small fraction of monolayer was observed on the glass substrate, which is shown in Figure 4.4, monolayer is capable to be produced on glass substrate as well.

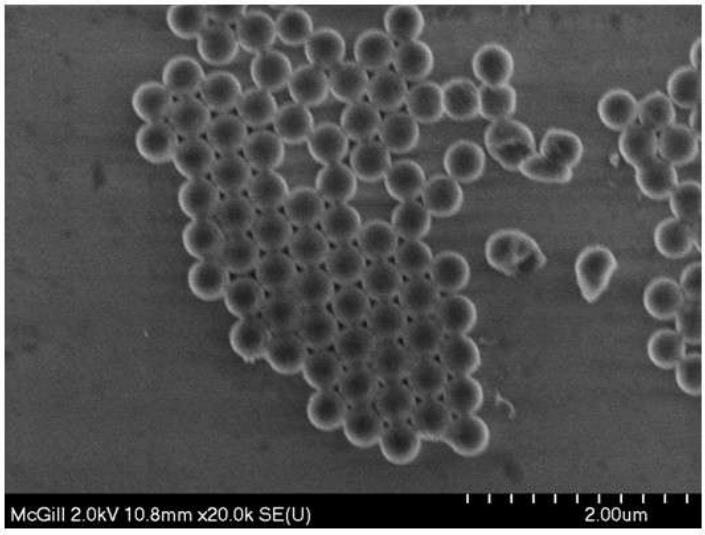

Figure 4.4: SEM of small fraction of hexagonal structure which was prepared with 420nm polystyrene on the glass substrate.

Polystyrene with the diameter of 920nm was deposited on glass substrate as well. The concentration of polystyrene suspension was still 1%, and syringe was used to remove the excess solution. Figure4.5 shows the SEM image of a small area of the monolayer which was prepared by the polystyrene with diameter of 920nm.

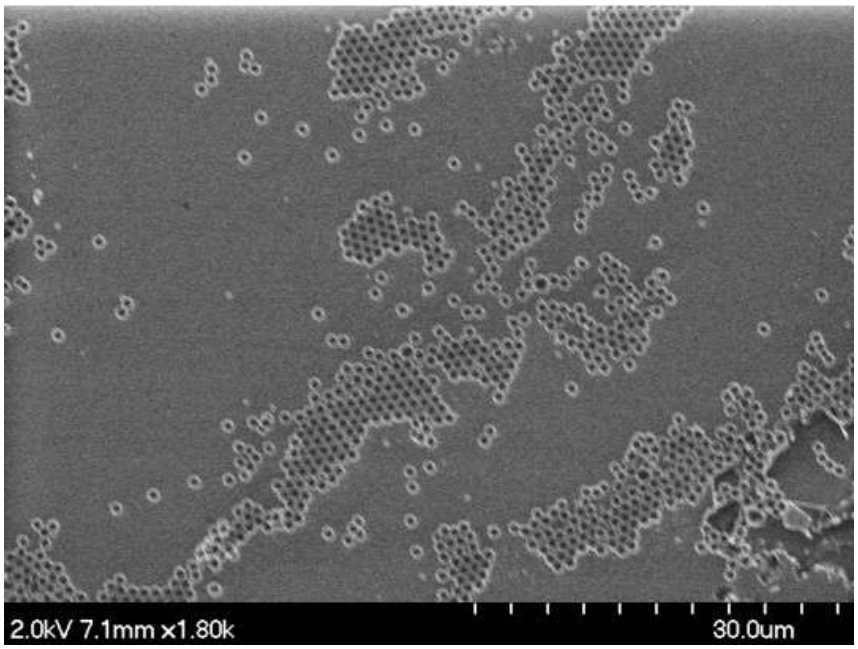

Figure 4.5: SEM image of a small fraction of monolayer which was prepared by polystyrene with the diameter of 920nm

It seems that with larger size of the polystyrene (920nm) is easier to produce monolayer nanoparticles on glass substrates compare to those with smaller size (420nm).

Using syringe to remove the excess liquid from the surface is not recommended as it may leave some cracks on the surface. Consequently, we use pieces of tissues to remove the solutions from the surfaces. Using this technique, we repeat the above method to produce monolyares of the polystyrene with diameter of 920 nm. The results were much better. The SEM image is shown in figure 4.6.

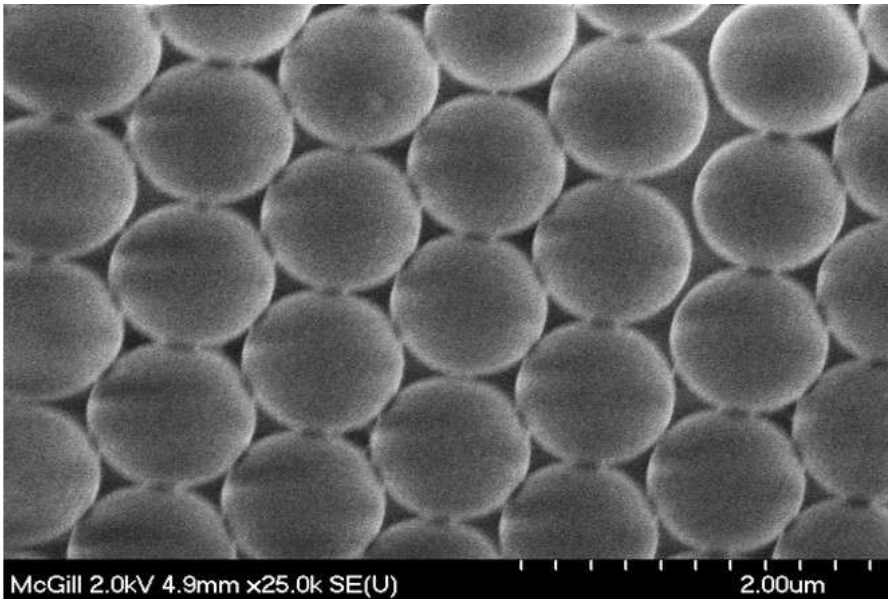

Figure 4.6: SEM image of regular, well ordered monolayer which was prepared by 920nm polystyrene on glass substrate

Monolayer cannot be formed by now when 420nm polystyrenes were used. One drop of the polystyrenes suspension was too much. Figure4.7 clearly shows that the amount of the suspension was the big is problem.

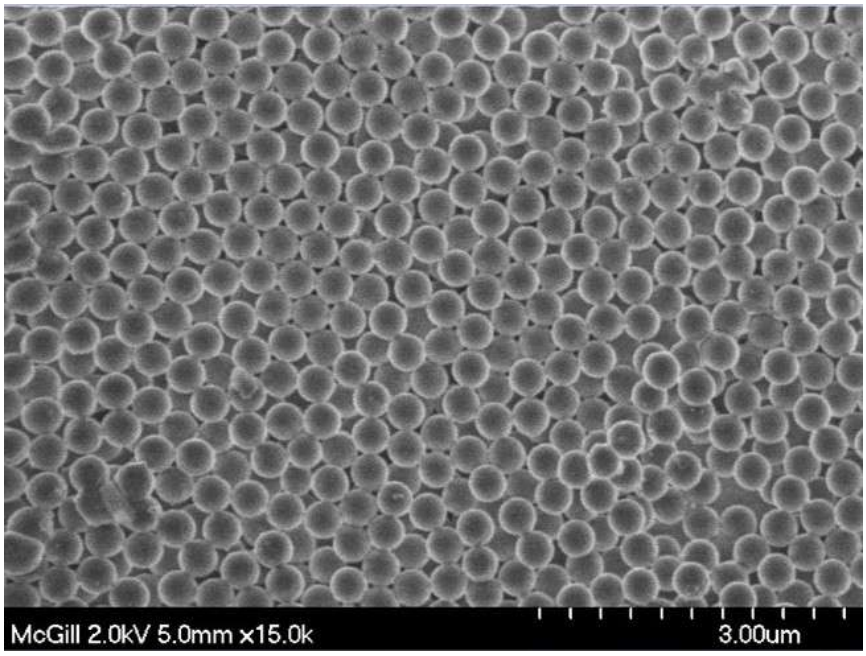

Figure 4.7: SEM image of multilayer which was prepared by excessive polystyrenes (the diameter is 420nm)

Nevertheless, monolayer can be achieved by decreasing the amount of the polystyrenes suspension (420nm) to half drop while remaining everything else exactly the same. The SEM image is shown as Figure 4.8.

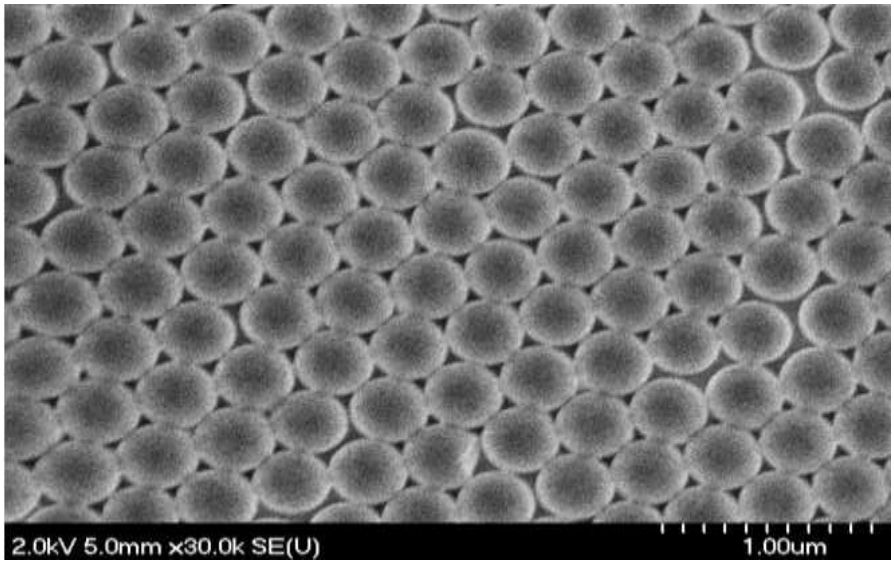

Figure 4.8 SEM image of monolayer which was prepared by polystyrene with diameter of 420nm

Further, we found out that a monolayer of polystyrene nanoparticles can be formed on samples of glass substrates without silanization, although the monolayer was more likely polycrystalline with numbers of grains boundary. The SEM image shown in figure 4.9 shows one of these samples.

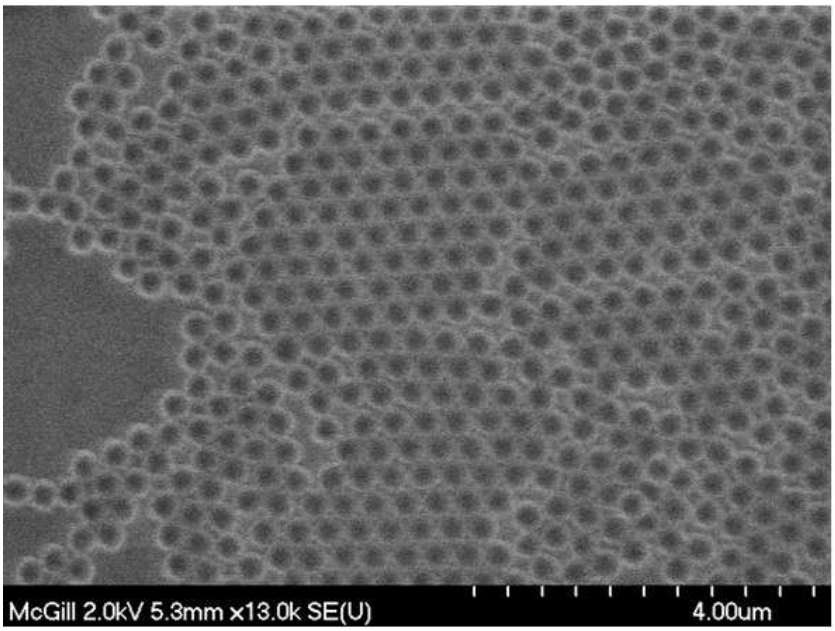

Figure 4.9: SEM image of the monolayer which was prepared on a non-silanized glass substrate.

As it is mentioned before, typical defect free monolayer can range from 10μm to 100μm. In this research, a large scale of monolayer can also be observed, as shown in Figure 4.10. In general, nanosphere lithography technique is powerful to produce regular, almost homogeneous arrays of monolayer.

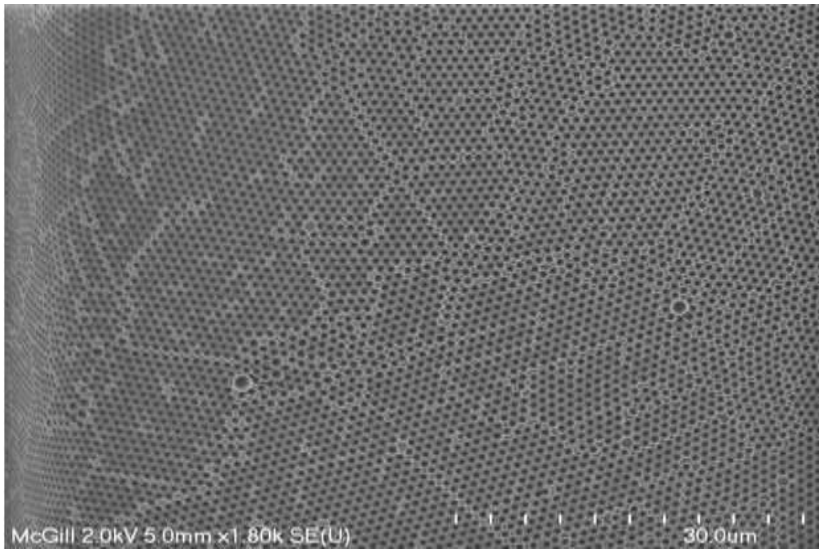

Figure 4.10: SEM image of large scale monolayer which was prepared by 920nm polystyrene on glass substrate

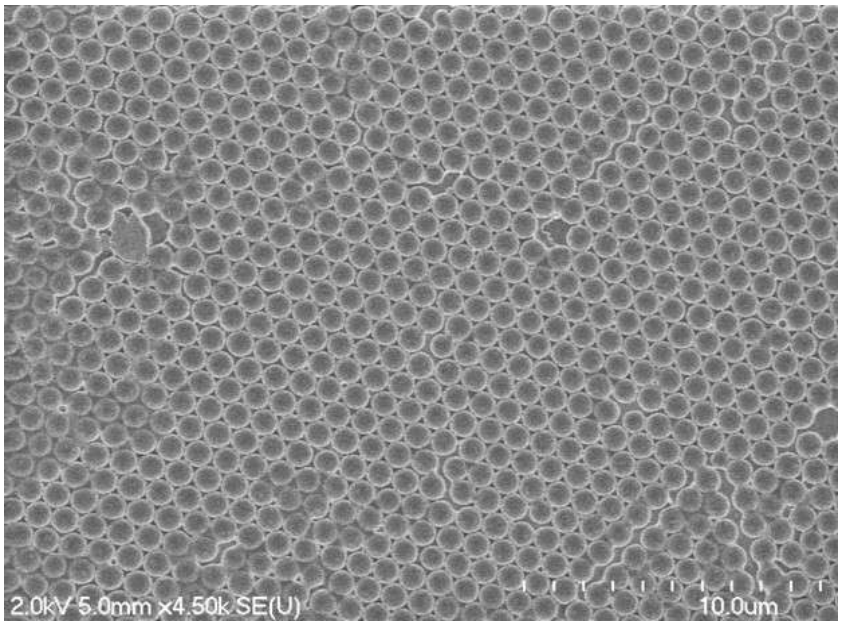

Figure 4.11: SEM image of the defects appear in the monolayer of nanoparticles.

However, there were still some defects. In Figure 4.11, defects like dislocation, missing a sphere can be observed, meanwhile, some defects which were resulted from the size difference of the polystyrene.

Meanwhile, two other methods were tried in this research to obtain monolayer:

1) vertically placing the substrates in a vial

2) lifting the substrates up to a slight angle

In the vertically placing method, substrates were placed in a vial vertically after polystyrene suspension was well spread on top of the surface, and let the samples dry at room temperature. Figure 4.12 shows the SEM image of the layers which were prepared by this method.

Figure 4.12 clearly shows that on the upper part of the substrate, very few polystyrene were attached to the substrate while on the lower part of the substrate, polystyrenes gathered around the bottom of the substrate and aggregated, forming polymer. Therefore, monolayer cannot be formed by this method. It might due to the gravity. Gravity dominated when capillary force tried to guide polystyrene to the right position to form hexagonal structure, and it eventually drove most of the polystyrene slid down to the bottom of the substrate and aggregate. What's more, gravity make polystyrene suspension quickly flow across the substrate surface, which might not be capable to offer enough time to polystyrene to form the hexagonal structure.

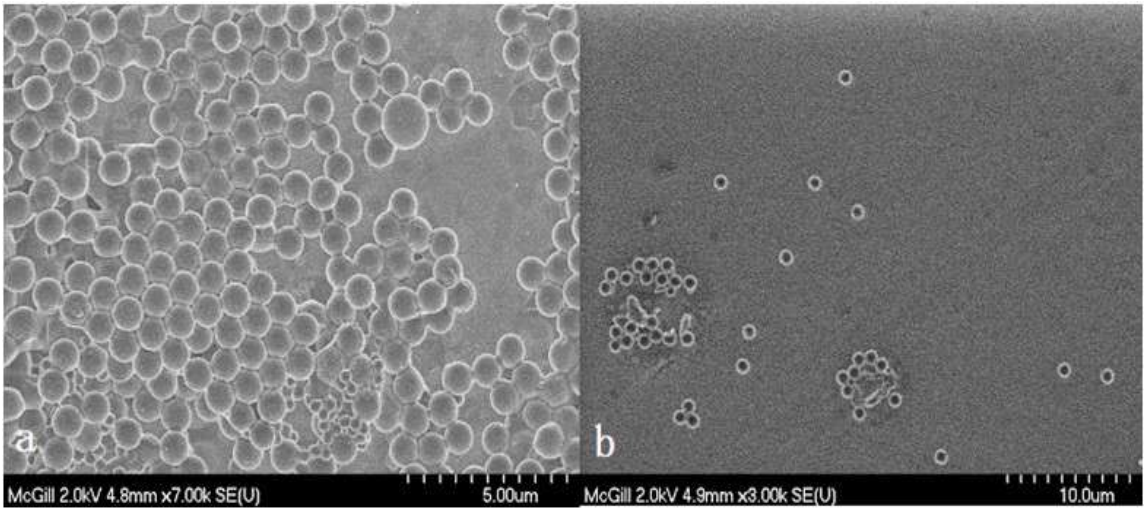

Figure 4.10: SEM image of a) polystyrenes which were attached on the lower part of the substrate and b) polystyrene which were on the upper part of the substrate.

In another method, the sample was titled with a small angle. One drop of polystyrene suspension and one drop of surfactant were placed on the surface just like the other experiments, solution slid down to the bottom of the sample and dried out..

In this experiment, polystyrenes suspension slowly slid down to the lower part of the substrate and aggregated, forming a multilayer of nanoparticles. A whole drop of suspension was too sufficient for a certain area of the substrate. A future work should be done to improve this procedure. Combining with taking out the excess solution might solve this problem and eventually get monolayer. Table 4.1 lists the condition when monolayer can be formed.

Table 4.1: Combination of various parameters to produce monolayer of nanoparticles on different substrates.

Size of the polystyrene	Substrates	Salinized	Composition	Taking out the excess solution by	Result	comments
420nm	Glass	Yes	0.5 drop of suspension +1 drop of surfactant	tissue	Large scale of monolayer can be formed	
920nm	Glass	Yes	1 drop of suspension +1 drop of surfactant	Tissue	Large scale of monolayer can be formed	
420nm	Silicon	No	1 drop of suspension +1 drop of surfactant	Syringe	Large scale of monolayer can be formed	
420nm	Glass	Yes	1 drop of suspension +1 drop of surfactant	Tissue	Multilayer can be formed	Suspension is too sufficient
420nm/920nm	Glass	No	0.5/1 drop of suspension +1 drop of surfactant	Tissue	Monolayer can be formed	Less scale and it's more like polycrystalline

4.4 Deposition of Nanoparticles and Morphology of Nanostructures

The monodisperse nanometre polystyrenes enclose interspaces with approximately 26% void in volume, in which the nanoparticles or metal plasma are easily infiltrated [48]. Substrates which were covered by well ordered monolayer were either put into a sputtering machine for gold thin film deposition or immersed in silver colloid solution for silver nanoparticles deposition.

4.4.1 Gold Thin Film Deposition on Substrates and its Morphology of Nanostructure

Substrates which were covered by well ordered monolayer were put in the chamber of sputtering machine for the gold thin film deposition. The working voltage was 0.7KV and the plasma flow was 80. Inert nitrogen gas was the working gas. Eventually, the thickness of the thin film is 25nm.

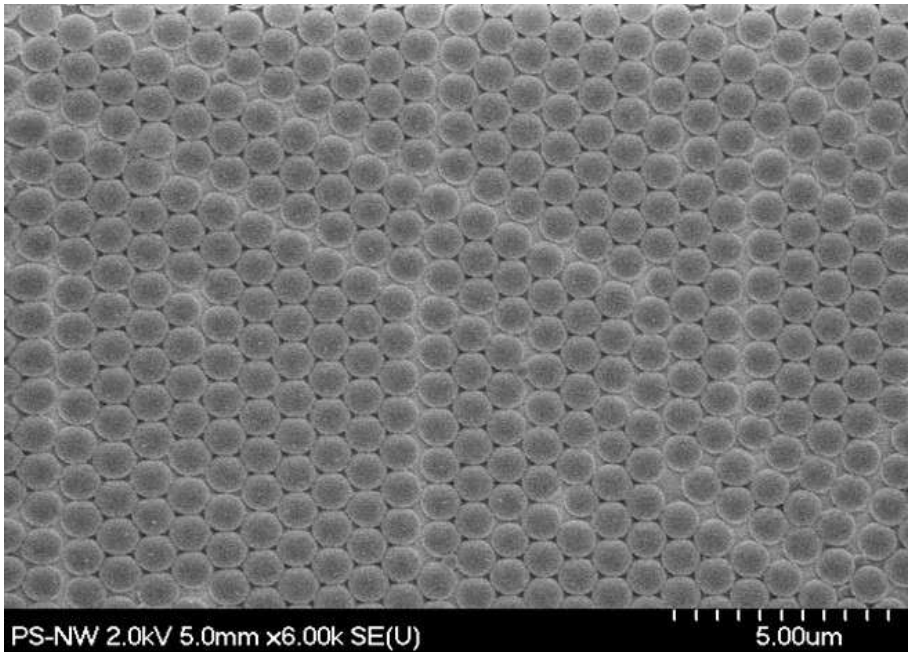

Figure 4.11: polystyrene monolayer covered by a thin film of gold and the thickness of the thin film is 25nm

After the whole substrate was covered by thin film of gold, shown as Figure 4.11, the polystyrene particles were removed from substrates by dissolving them in ethanol with the aid of sonication for 10 seconds. Subsequently, the substrates immersed in chloroform solution for 5 seconds. Triangular or nanorings gold structures produced by this approach were observed through SEM.

Both triangular nanostructures and nanorings were found in the samples which were prepared by polystyrene with the diameter of 920nm. Figure 4.12 depicts the SEM image of triangular nanostructures which are produced from a sample prepared with 920nm polystyrene spheres. The thickness of the triangular structure is 25nm in average. This image contains areas of well-defined triangular nanostructures.

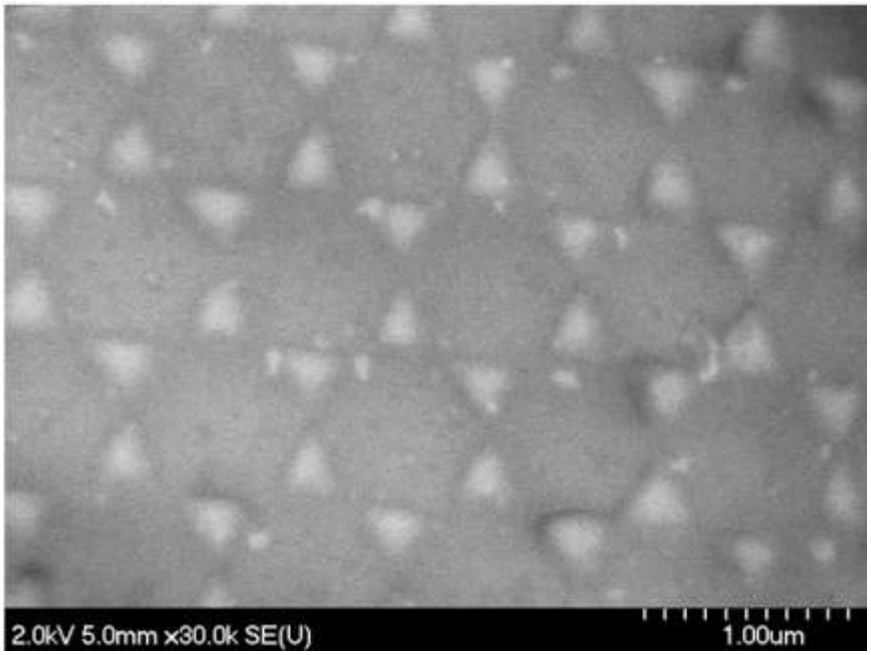

Figure 4.12: SEM image of triangular nanostructures which are produced from a sample prepared with 920nm polystyrene spheres.

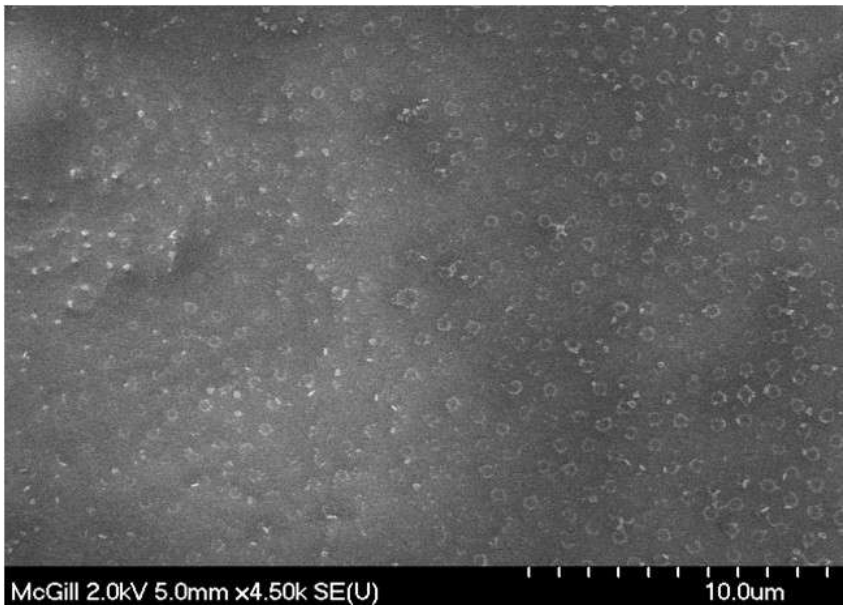

Figure 4.13: SEM image of nanorings which were prepared by 920nm polystyrene on glass substrate

Figure 4.13 is an SEM image of nanorings which are fabricated from a sample prepared with 920nm polystyrene. Compared to triangular nano structures, the probability of obtaining nanoring structure is quite small for a sample which was prepared with 920nm. In this research, many samples were prepared to study the morphology of the structures; only two of them appeared to have nanorings structures. The diameter of these nanorings is 400nm in average and they are about 920nm apart from each other.

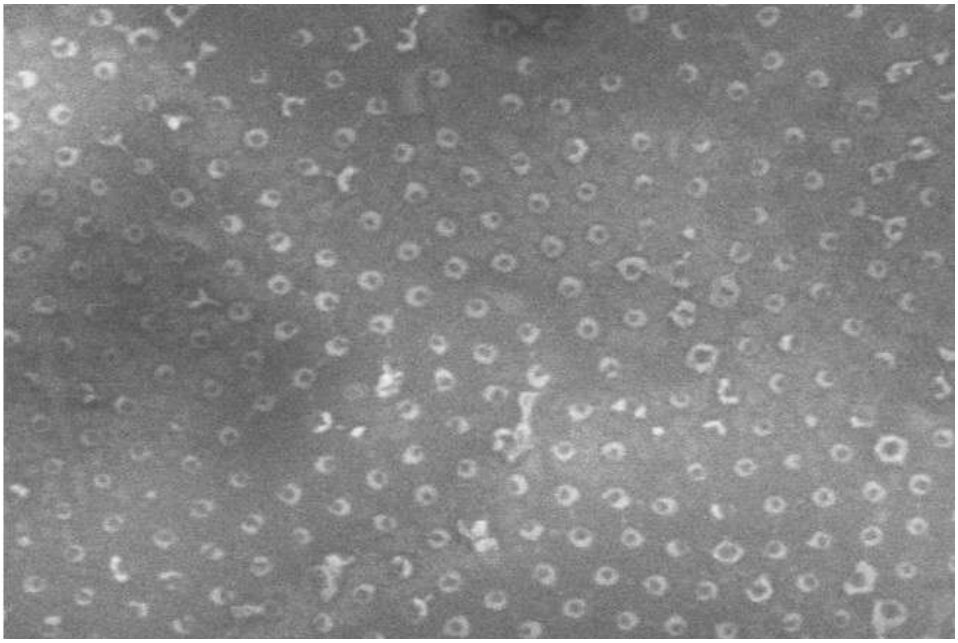

Figure 4.14: SEM image of nanorings which were prepared by 420nm polystyrene on glass substrate

Figure 4.14 shows the SEM image of nanorings from a sample which is prepared by the polystyrene with the diameter of 420nm. The thickness of the deposited gold metal was about 25nm. Unlike the samples prepared using 920nm polystyrene, all of these samples can only fabricate nanorings structure. These nanorings are well order, 420nm apart from each other and with the diameter of 200nm in average. A likely explanation of

the formation of nanorings is that the interspaces among the 420nm polystyrene microspheres are smaller than that among the 920nm polystyrene microspheres, and this gets more difficult for gold atoms/ions to well deposit into the interspace among the polystyrene microspheres. Most of them are stuck and stay on top of the polystyrene microsphere monolayer. In addition, pure gold is soft and easy to deform as the bond length of gold is 1.34Å which is not strong enough. Given this, some gold ions/atoms might slid down to the bottom of the polystyrene microspheres other than not stay bonded to each other on the top surface of polystyrene. Therefore, ring shape structure formed around the foot of the sphere. Meanwhile, structure which is shown as Figure 4.15 is also observed on the same sample. Those nanopores were formed by filling all available interspaces of the polystyrene sphere with gold atoms/ions.

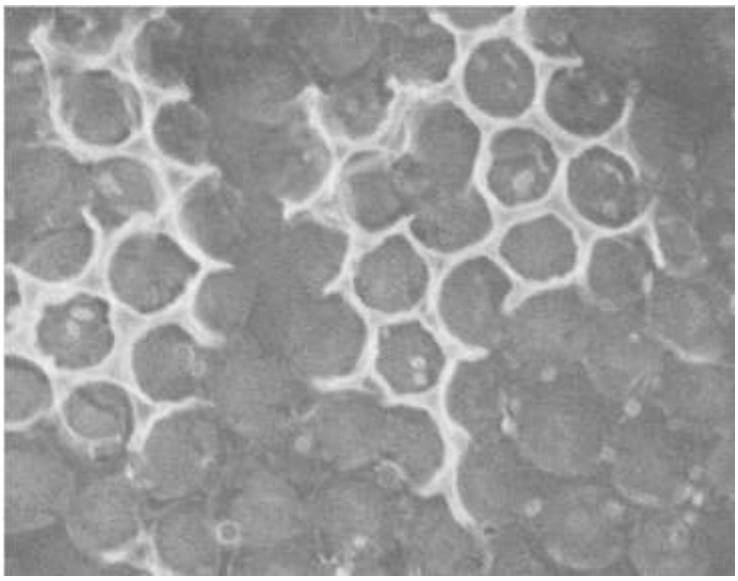

Figure 4.15: SEM image of another ring-like structure which was prepared by 420nm polystyrene during the sputtering process

Adjusting the thickness of metal thin film to 5nm, the result was quite different and it is shown as Figure 4.16.

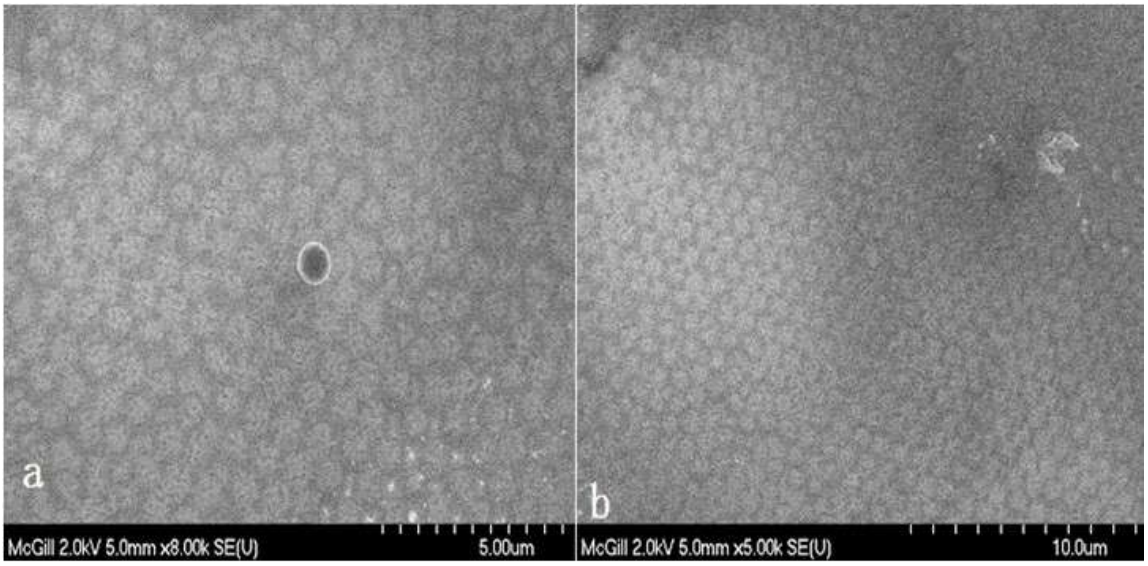

Figure 4.16: SEM image of the structure after removing the polystyrenes (the thickness of sputter thin film is around 5nm)

Figure 4.16 depicts that when decreasing the thickness of the gold thin film to 5nm, no triangular nanostructures or nanorings can be observed after removing the polystyrenes. However, the trace of well-ordered, hexagonal monolayer was left. Hence, 5nm might not be enough for the deposition procedure.

Though monolayer can be formed on those non-silanized glass substrates, no metal structure can be found after removing the polystyrenes. It also proves that the long pair of the nitrogen atom in amino group indeed assists in adherence between metal nanostructures and glass substrate.

4.4.2 Silver Colloids Deposition on Monolayer

Triangular structures or nanorings were also expected by immersing the substrates covered with polystyrenes monolayer into silver colloids solution. Few drops of silver colloid suspension were added on the horizontally placed glass substrates which were covered by polystyrene monolayer. The samples were dried either at the room temperature or at 50^0C in an oven. The same removal procedure described before was applied for removing the polystyrene particles. Polystyrene particles were dissolved in ethanol with sonication for 10 seconds followed by 5 seconds immersing in chloroform solution.

Silver colloids produced in the sodium citrate solution method (method I) seemed to be unfavoured to fill the inter-space between the polystyrene spheres. For those samples which were dried at 50^0C in the oven, no silver colloids were found gathering among or at the bottom of the polystyrenes. High temperature might have contributed to both the activity of the metal colloids and evaporation rate; the faster the solution was evaporating, the less time was left for colloids moving freely to settle down among the PS.

As it is shown in figure 4.17, for the samples which were dried up at room temperature, although the inter-space between the spheres was large enough to let silver colloids to pass through (we could calculate the diameter of the inter-space according to Equation 2.4 and this is approximately 214nm for D equalling to 920nm; while the diameter of the silver colloids in average is 30~40nm) nevertheless, silver colloids stayed on top of the spheres.

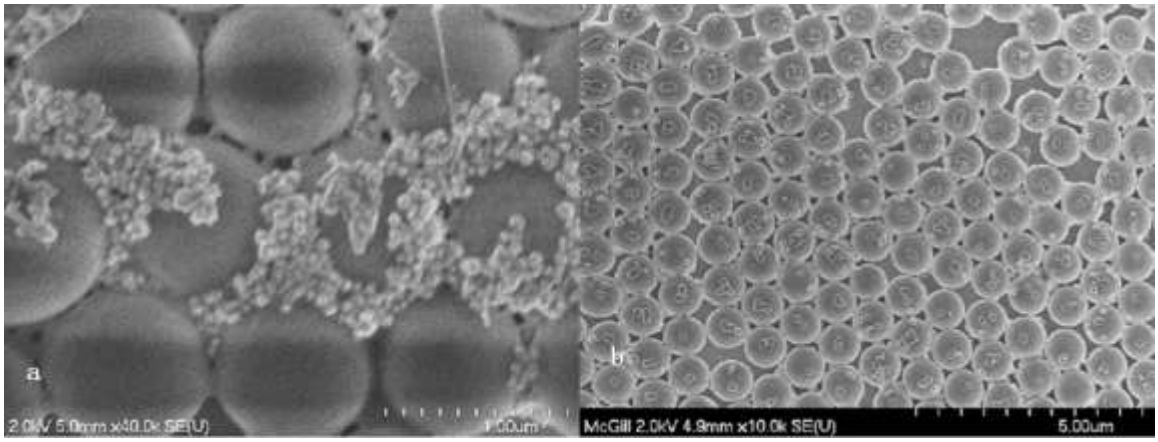

Figure 4.17: SEM image of silver colloids on top of the polystyrene spheres.

Nevertheless, not all of the silver colloids stayed on top of the spheres, some structures which are shown in Figure 4.18 and Figure 4.19 were also observed in the research. In these two figures, silver colloids fully filled in the inter-space among these polystyrene.

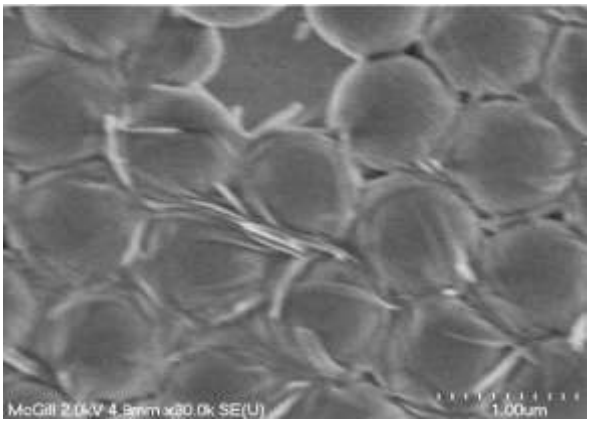

Figure 4.18: SEM image of monolayer which was filled by silver colloids.

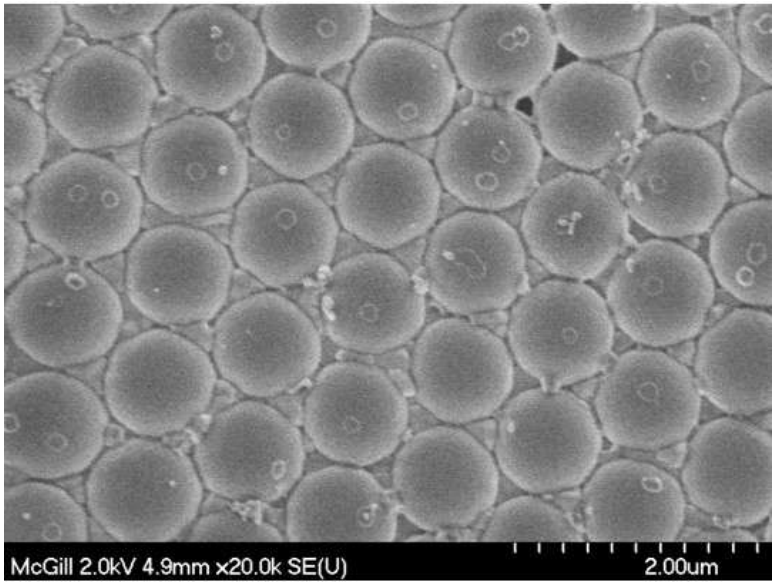

Figure 4.19: SEM image of monolayer which was fully filled by silver colloids.

However, only a very small portion of monolayer was fully filled by silver colloids. Improvements may happen by controlling the temperature during the evaporation process. No triangular nanostructures or nanorings were found after removing the polystyrenes.

Table 4.2 lists the result of the metal structures can be obtained with different metal deposition methods in this research work.

Table 4.2: list of the result of the metal structures can be gotten with different size of polystyrene and thickness of the thin film

Size of the polystyrene	Thickness of the thin film	Method	Structure
420nm	25nm	Sputtering thin gold film	Nanorings
920nm	25nm	Sputtering thin gold film	Mostly: triangular particles Occasionally: nanorings
920nm	5nm	Sputtering thin gold film	Only trace of the hexagonal form can be found
920nm	Not clear	Silver colloids solution	Nothing

Chapter 5: Results and Discussion

5.1 Discussion of Absorption Spectrum

In this research, we successfully fabricated nanostructures made of triangular and nanorings componenets. Structures with triangular and nanorings components were produced by depositing self-assembled, crystalline monolayers of polystyrenes nanoparticles on glass and silicon wafers.

As we introduced in the previous chapter, LSPR arises at specific wavelengths when the frequency of incident photon is resonant with the collective oscillation of the conduction electrons in the metallic nanostructures and it's very dependent on the size, shape, degree of coupling of the nanostructures, inter-spacing, and dielectric properties of the material, as well as the dielectric properties of the surrounding; the extinction maximum (λ_{max}) of nanostructures will shift when the local environment changes and that is the basis of biosensors which are based on LSPR to detect. In this research, UV-vis spectroscopy was used to measure the extinction and the shift of the extinction; the shift of the extinction represents the sensitivity of a sensor. UV-vis spectrum shows different properties which is very dependent on the size, shape and concentration of the nanostructures.

In order to calculate the sensitivity of the nanostructures, the absorption spectrum was measured for each sample in Environmental Engineering Laboratory in Concordia University. Samples were erected in a glass vial which was full of de-ionized water and the absorbance spectra of the samples were recorded in the visible region.

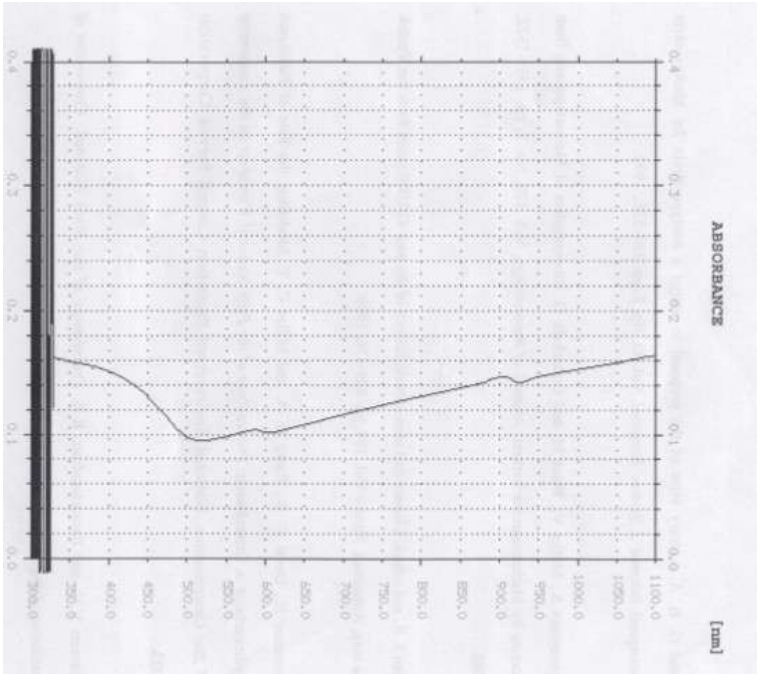

Figure 5.1: Uv-vis spectrum of metal thin film with the thickness of 25nm

Figure 5.1 depicts the Uv-vis spectrum of a thin metallic film which has the thickness of 25nm, and it shows that no extinction peak was found in the wavelength ranging from 300nm to 1100nm. The surrounding environment was de-ionized water. The purpose of measuring the absorption spectrum of the gold thin film was expected to set a reference to that of the metal nanostructures, and to observe the resonance between nanostructures and light.

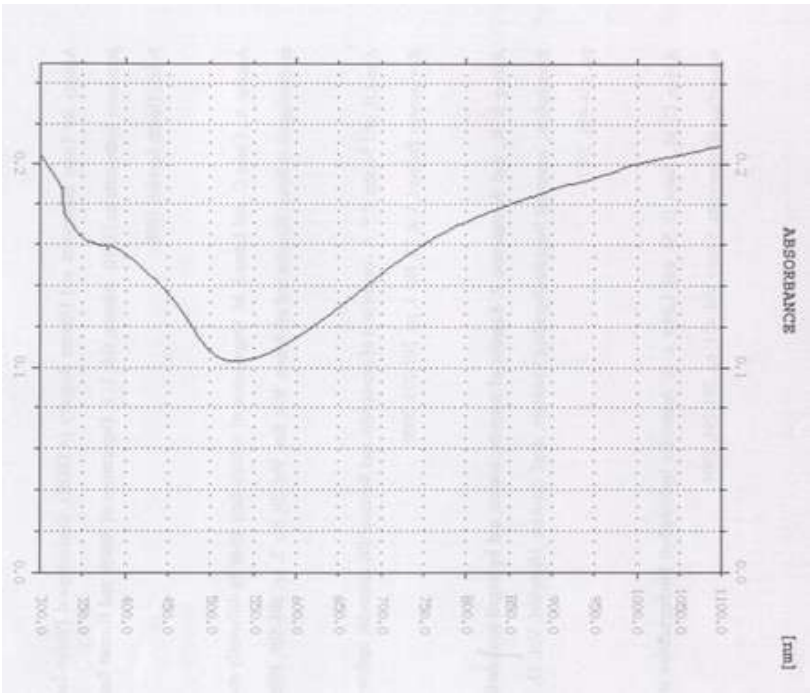

Figure 5.2: Uv-vis spectrum of triangular nanotructures which were prepared by 920nm polystyrene

Figure 5.2 reveals the absorption spectrum of the sensor with triangular structures produced by the 920nm polystyrene, the average diameter of these triangular nanostructures is 210nm. Still, the surrounding environment is de-ionized water.

Apparently, no extinction peak was found in the figure shown above. However, as mentioned before, the LSPR extinction peak will shift to the longer wavelength as the size of nano structure increase. The size dependent property corresponding to the Near and Mid-Infrared extinction measurement were described in the research of Dr. Richard P. Van Duyne [49]. For the silver triangular nanostructures which have the average diameter of 240nm, the extinction peak appeared at the wavelength of 1125nm [49]. Figure 5.3 shows the extinction of the well ordered nanostructure array.

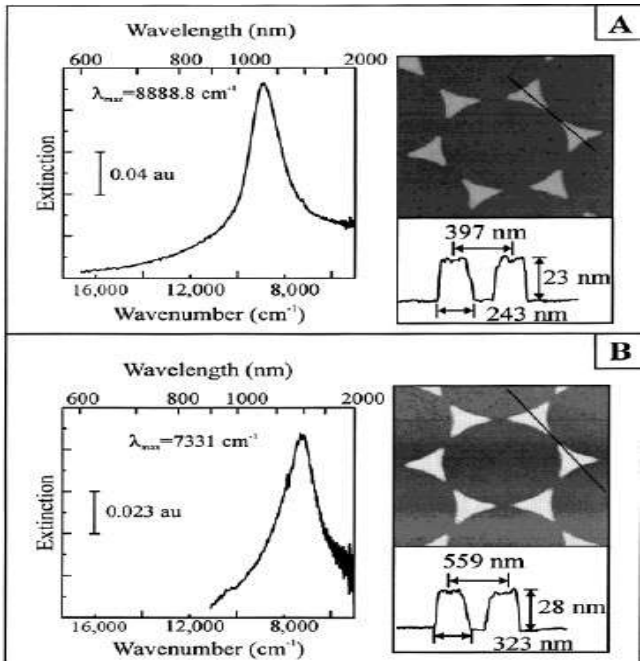

Figure 5.3: UV-vis extinction spectrum of Ag triangular array [49]

Though gold particles and silver particles have different absorption band and different extinction peak, still, for gold particles, the extinction peak will shift to Near Infrared area as the size of the particle increases. What's more, the absorption band of gold nanostructures occurs at a longer wavelength compared to that of silver nanostructures with a competitive size. Therefore, for these reasons the extinction peak for the devices fabricated in this work might appear far beyond the maximum wavelength (1100nm) that can be measured in our laboratories.

Nanorings exhibit pronounced extinction peaks at much larger wavelength, a typical extinction peak is in the range of 1000-1500nm [50].

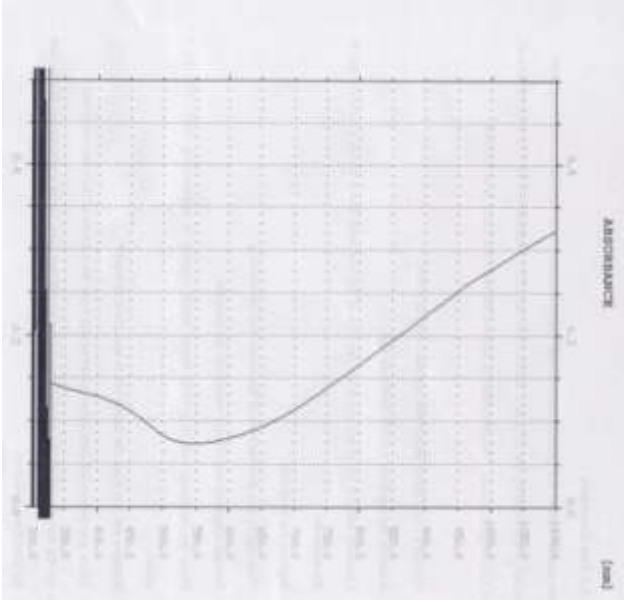

Figure 5.4: Uv-Vis spectrum of nanorings prepared by the polystyrene with the diameter of 420nm

Unfortunately, similar to the Uv-vis spectrum of triangular structures, no extinction peak was found in the Figure 5.4 and this might be due to the limitation of our instruments.

Chapter 6: Conclusion and Future work

In this work, nanostructures such as nanorings and triangular particles are produced with the help of monolayer which was prepared by nanosphere lithography. Nanosphere lithography technique provides a simple, convenient, low-cost, high-throughput method to form 2D array of nanostructure from several materials on the surfaces of a series of substrates.

Monolayer was formed by self assembly deposition through spreading the polystyrenes suspension on an amino-silane activated glass substrate. Monolayer acts as a template to provide the basic structure of the nanostructure and determines the size, shape and inter-space of the nanostructure. Gold plasmon was sputtered to the surface of the monolayer and some of them slit down to the bottom of the polystyrenes or aggregated in the interspaces of the spheres. After the polystyrene spheres were removed by being dissolved in ethanol solution with the help of sonication then followed by chloroform solution, a uniform, well ordered structure was obtained.

Nanorings can be produced with the monolayer which was prepared with comparative small size of polystyrene (420nm) and triangular nanostructures can be produced with the larger size of polystyrene (920nm), meanwhile, nanorings can be produced in a very small possibility with the larger size polystyrenes. This might be due to the fact that the bond of gold is not strong and easy to deform, besides, the spaces between the small size polystyrenes are smaller than those between the larger size polystyrenes. It may causes difficulty for gold plasmon to pass through.

In addition, silicon substrates are ideal material to grow monolayer on them.

During the process of preparing the monolayer, one method (lift the substrate up to a slight angle and let the solution dry without taking excess solution) was tried but failed. Future work might require taking out the excess solution while still lifting up the substrate to a slight angle. In this case, polystyrene suspension may slowly cover all the substrate and leave the polystyrene spheres enough time to deposit at those sites which were expected. Meanwhile, taking out the excess solution with tissue at the lower edge of the substrate, this would not damage the surface of the layer.

In the future, etching technology can be combined with the nanosphere lithography to prepare nanostructure. The size of the structure and distance between the structures are determined by the size of the polystyrenes which were used to produce the monolayer; however, with the aid of etching technology, the size of the nanostructure can be of multiple choices. In a certain area of substrate, the size of the polystyrenes determines the concentration of the nanostructures; meanwhile, the concentration of the nanostructure partially determines the sensitivity and selectivity of a biosensor. Therefore, sensitivity and selectivity of sensors can optimize by changing the size of the polystyrenes and consequently changing the size of the nanostructures.

In addition, due to the limitation of the equipment in our lab, no extinction peak can be measured in this research; however, extinction peak is dependent on the size of the nanostructure which can be controlled by adjusting the size of the polystyrene. Therefore, the extinction peak will shifts to visible and Near-infrared range if only the size of

triangular structures is smaller than that of the triangular nanostructures which was prepared with 920nm polystyrenes.

Reference

1. http://www.nano.gov/html/facts/whatIsNano.html. (August 2, 2010)

2. http://en.wikipedia.org/wiki/List_of_nanotechnology_applications.(August 10, 2010)

3. http://en.wikipedia.org/wiki/Quantum_well. (August 10, 2010.)

4. http://www.nanosens.nl/focus.htm.(August 2, 2010)

5. http://en.wikipedia.org/wiki/Quantum_dot.(August 4, 2010)

6. Kourosh Kalantar-zadeh, Benjamin Fry. Nanotechnology-Enabled Sensors. (springer, Melbourne, Victoria, Australia, 2008)

7. http://en.wikipedia.org/wiki/Nanoparticle.(August 4, 2010)

8. Jon S. Wilson. Sensor technology handbook. (Elsevier, Amsterdam ; Boston, c2005).

9. T. Vo-Dinh, B. Cullum, Anal. Chem., **366**, 540 (2000)

10. http://en.wikipedia.org/wiki/File:Light-wave.svg.(October 10, 2010)

11. H.Raether. Surface Plasmons on Smooth and Rough Surfaces and on Gratings . Surface Plasmons on Smooth and Rough Surfaces and on Gratings . (Springer-Verlag Berlin, 1988).

12. Boardman, A.D. Electromagnetic Surface Modes . Electromagnetic Surface Modes . (Wiley, Newyork, 1982).

13. Xin hong and Fu-Jen Kao, applied optics, **43**, 14 (2004)

14.Zhao.J, Zhang. X.,Yonzon. C.R, Haes,A.J, Van Duyne. R.P, Nanomedicine, **1**(2), 219-228 (2006)

15. S. Lind, M. A. El-Sayed, Int. Rev. Phys. Chem, **19**, 409 (2000)

16. Kribig,U. and Vollmer, M. Optical properties of metal clusters. (Springer-Verlag, Berlin, 1995)

17. N, Nidth, and C, Ashutosh, Anal.Chem, **76**, 5370-5378 (2004)

18. D.A. Stuart, A.J. Haes, C.R. Yonzon, E.M. Hicks and R.P. Van Duyne, IEE Proc.-Nanobiotechnol, **152**, 1(2005)

19. Jung, L.S., and Campbell, C.T, J. Phys. Chem. B, **104**,11168–11178 (2004)

20.Jung, L.S., Nelson, K.E., Stayton, P.S., and Campbell, C.T, Langmuir, **16**, 9421–9432 (2000)

21.Rao, J., Yan, L., Xu, B., and Whitesides, G.M, J. Am. Chem. Soc., **121**, 2629–2630 (1999)

22. Berger, C.E.H., Beumer, T.A.M., Kooyman, R.P.H., and Greve, J., Anal. Chem., **70**, 703–706 (1998)

23. Heaton, R.J., Peterson, A.W., and Georgiadis, R.M., Proc. Natl. Acad. Sci., **98**, 3701-3704 (2001)

24. McFarland, A.D., and Van Duyne, R.P., Nano Lett., **3**, 1057–1062 (2003)

25. Y. Dirix, C. Bastiaansen, W. Caseri and P. Smith., Adv. Mat., **11**, 223-227 (1999)

26. Sanchez, E. J., Novotny, L., Xie, X.S., Phys, Rev. Lett., **82**, 4014-4017 (1999)

27. Nie, S.; Emory, S.R.,Science, **275**, 1102-1106 (1997)

28. Bauer, G.; Pittner, F.; Schalkhammer, T., Mikrochim. Acta, **131**, 107-114 (1999)

29. F. Fida, L. Varin, S. Badilescu, M. Kahrizi and Vo-Van Truong., Plasmonics, **4**, 201-207 (2009)

30. John c.Hulteen, David A. Treichel, Matthew T. Smith, Michelle L. Duval, Traci R. Jensen, and Richard P, Van Duyne., J. Phys. Chem. B, **103**, 3854-3863 (1999)

31.Christian Gigault, Kari Dalnoki- Veress, John R. Dutcher, Journal of Colloid and Interface Science, **243**, 143-155 (2001)

32.Simona Badilescu, Nader Seirafianpour, Ahmad-Reza Hajiaboli, Yahia Djaoued, Mojtaba Kahrizi, P. V. Ashrit, Vo-Van Troung, J Mater Sci: Mater Electron, **18**, 383-387, (2007)

33. J. Zhang, Z.-L. Wang, J. Liu, S. Chen, and G.-Y. Liu. Self-assembled nanostructures. (Kluwer Academc/Plenum Publishing, New York, USA, 2003).

34. Charles P. Poole, Jr. Frank J. Owens, Introduction to Nanotechnology. (Wiley, 2003)

35. S.-R. Yeh, M. Seul, B.I.Shraiman., Nature, **386**, 57 (1997)

36. Mitropoulos, A. Ch., Engineering Science and Technology Review **2**(1), 28-32 (2009)

37. N. D.; Velev, O. D., Kralchevsky, P. A., Ivanov, I. B., Yoshimura, H., Nagayama, K. Nature, Nature, **361**, 26 (1993)

38. Richard P. Van Duyne, Amanda J. Haes, and Adam D. McFarland, Physical Chemistry of Interfaces and Nanomaterials II, **5223**,197

39. G.U. Lee, D.A. Kidwell and R.J. Colton, Langmuir, **10**, 354-357 (1994)

40. T. Nakagawa, Tohru; Ogawa, Kazufumi; Kurumizawa, Toshimitsu, Journal of vacuum Science & Technology B, **12**, 2215-2218 (1994)

41. E.L.Florin, M.Rief, H.lehmann, M. Ludwig, C.Dornmair, V.T. Moy, and H. E. Gaub, Biosensors & Bioelectronics **10**,895-901 (1995)

42. J. W. Zhao and K. Uosaki. Langmuir **17**, 7784-7788 (2001)

43. McGovern, M.E.; Kallury, K.M.R.Thompson, M.., Langmuir, **10**, 3606-3614 (1994)

44. Enders,D.;Nagao,T.;Pucci,A.;Nakayama,T., Surf.Sci., **600**, 71-75 (2006)

45. Kooij,E.S.;Brouwer,E.A.M;Wormeester,H.;Poelsema,B., Langmuir, **18**, 7677-7682 (2002)

46. Howarter, J. A.; Youngblood, J.P., Langmuir , **22**, 11142-11147 (2006)

47.Fillip Fredirix, Jean-Michel Friedt, Kang-Hoon Choi, Wim Laureyn, Andrew Campitelli, Dirk Mondelaers, Guido Maes, and GUstaaf Borghs, Anal. Chem., **75**, 6894-6900 (2003)

48. Daniel S. Ramundo, Francisco J. R. Fernandez and Walter J, Salcedo, Journal integrated circuits and systems, **1**(3), 39 (2006)

49. Traci R. Jensen, Michelle Ducal Malinsky, C.L. Haynes, and R.P. Van Duyne: Nanosphere Lithography. J.Phys. Chem.B, **104**, 10549 -10556 (2000)

50. J. Aizpurua, L. Blanco, P. Hanarp. D.S. Sutherland, M. Kall, Garnett W. Bryant, F.J.Garcia de Abajo., Quantitative spectroscopy.